https://doi.org/10.5194/egusphere-2026-3135
Preprint. Discussion started: 7 July 2026

Astronomical pacing and impact of the Middle Maastrichtian warming event on the Maastrichtian upwelling system of the southern Neo-Tethys Ocean margin (Jordan)

Jihede Haj Messaoud[1]*, Maria Ardila-Sanchez[1], Khalil, Ibrahim[2], Israa Abu-Mafouz[3], Volker Vahrenkamp[1], Frans van Buchem[1]**

[1] King Abdullah University of Science and Technology, Thuwal, Saudi Arabia

[2] The Hashemite University, Zarqa, Jordan

[3] King Fahd University of Petroleum and Minerals, Dhahran, Saudi Arabia

*Corresponding author: jihede.hajmessaoud@kaust.edu.sa

**Co-corresponding author: frans.vanbuchem@kaust.edu.sa

Abstract

The southern NeoTethys Ocean margin was the site of one of the most organically rich Early Maastrichtian global upwelling systems, with organic matter concentrations reaching>20% TOC, which came to an abrupt end in the Late Maastrichtian, when sedimentation changed to pure chalk deposits. The integration of biostratigraphy, climate and depositional environment proxies, and cyclostratigraphy demonstrated that this change from organic to carbonate-dominated productivity occurred around the Early-Late Maastrichtian and was time equivalent to a climatic change from cooler to warmer conditions. The smaller scale productivity variations were paced by the eccentricity modulated precession orbital cycles. The integration of calcareous nannofossil and dinoflagellate cyst biostratigraphy, radiolarian paleoecology, stable isotope geochemistry ($\delta^{13}C_{carb}$, $\delta^{13}C_{org}$, $\delta^{18}O$ and $\delta^{15}N_{org}$), and organic geochemical proxies from two closely spaced shallow cores (139 m and 71 m thickness) in Central Jordan were used to reconstruct the evolution of the

https://doi.org/10.5194/egusphere-2026-3135
Preprint. Discussion started: 7 July 2026

Maastrichtian upwelling system developed along the Levant margin of the southern NeoTethys Ocean. Integrated biostratigraphic and chemostratigraphic data constrain deposition of the oil shale interval to the Early Maastrichtian (72.7–68.2 Ma), representing ~4.5 Myr of accumulation with sedimentation rates of ~1.5–2.2 cm kyr^{-1}. Pronounced lithological and geochemical cyclicity reveals a dominant precession signal modulated by short eccentricity (~100 kyr), suggesting that eccentricity-paced insolation forcing regulated migration of the Intertropical Convergence Zone (ITCZ), regional wind intensity, and coastal upwelling strength. These orbitally forced changes controlled nutrient delivery, marine productivity, as expressed in the calcareous nannofossil, dinoflagellate cyst, and radiolarian assemblages, and cyclic accumulation of organic-rich sediments. Combined $\delta^{13}C_{carb}$, $\delta^{13}C_{org}$, and calcareous nannofossil records place the Middle Maastrichtian Carbon Isotope Event within the upper part of the oil shale succession. $\delta^{18}O$ trends and nannofossil assemblage variations indicate cooling during the Early Maastrichtian, followed by warming during the early Late Maastrichtian. Low total organic nitrogen values, elevated C/N ratios, depleted $\delta^{13}C_{org}$ values, and enriched $\delta^{15}N_{org}$ signatures indicate intense diagenetic recycling of nitrogen-rich organic matter under persistent oxygen-deficient conditions, likely involving denitrification within an expanded oxygen minimum zone. Our findings demonstrate the coupled influence of orbital forcing and climate change on upwelling dynamics, marine productivity, and biogenic sedimentation during the Early Maastrichtian.

1. Introduction

During the latest Cretaceous, the southern Tethys Ocean was characterized by an extensive and highly productive upwelling system that exerted a major control on marine sedimentation and paleoceanographic conditions. Similar to modern eastern boundary upwelling systems, this circulation regime promoted elevated biological productivity and the accumulation of organic-

https://doi.org/10.5194/egusphere-2026-3135
Preprint. Discussion started: 7 July 2026

rich, siliceous, and phosphatic sediments along the continental the Levant continental shelf (Ashckenazi-Polivoda et al., 2011; Beik et al., 2018; Bou Daher et al., 2015; Meilijson et al., 2014; Moshkovitz et al., 1983; Usman et al., 2025). Along the Northern Arabian Plate shelf margin, the interaction between this long-lived upwelling system and local tectonics of the Syrian Arc generated pronounced spatial variations in sedimentation, facies distribution, and organic matter accumulation across shelf basins (Bou Daher et al., 2015; Edelman-Furstenberg, 2009a), whereas in Jordan a more subtle role of local tectonics led to much less pronounced thickness variations (Kalifi et al., 2025). Upwelling intensity reached its maximum in Jordan during the Campanian–early Maastrichtian, leading to the deposition of the Al Hisa Phosphorites (AHP) Formation and the Muwacker Chalk Member (MCM) Formation, which is characterized by high TOC values and persistent dysoxic, anoxic, and euxinic bottom-water conditions (Giraldo-Gómez et al., 2018; Usman et al., 2025). The Maastrichtian was also a time of major climatic and oceanographic fluctuations superimposed on the long-term Late Cretaceous greenhouse-cooling trend. One of the most significant perturbations was the Middle Maastrichtian Event (MME; ~69.2–68 Ma), a global warming phase associated with a 2–4°C increase in ocean temperatures, reorganization of ocean circulation, and major paleoecological changes(Dubicka et al., 2024; Li & Keller, 1998). The MME coincided with the decline of inoceramid bivalves and reductions in rudistid communities, reflecting changes in productivity, water-column stratification, and deep-water circulation (Dubicka et al., 2024; Nifuku et al., 2009). Although this event has been documented globally across the Pacific, Atlantic, Indian, and Tethyan oceans (Chauris et al., 1998; Dubicka et al., 2024; Frank et al., 2005; Li & Keller, 1998; MacLeod, 1994; Nifuku et al., 2009; Razmjooei et al., 2020).

The Middle Maastrichtian Event (MME), a major ~1.2 Myr warming episode, has not been confidently recognized on the Arabian Plate owing to the lack of integrated isotopic,

https://doi.org/10.5194/egusphere-2026-3135
Preprint. Discussion started: 7 July 2026

biostratigraphic, and high-precision geochronological constraints. Consequently, its impact on the southern Tethyan upwelling system remains poorly understood. Assessing how this warming event and orbital-scale climate variability affected upwelling intensity, marine productivity, oxygenation, and organic matter accumulation is essential for evaluating the sensitivity of Late Cretaceous greenhouse oceans to climatic forcing. In particular, orbital-driven shifts in the position and intensity of the Intertropical Convergence Zone (ITCZ) may have influenced regional wind systems and, consequently, the strength of wind-driven upwelling along the southern Tethyan margin (e.g., Bou Daher et al., 2014). Maastrichtian organic-rich deposits in Jordan provide an exceptional archive for reconstructing palaeoenvironmental and palaeoclimatic changes along the southern Tethyan margin. Previous studies have shown that the organic-rich interval was deposited under highly productive marine conditions dominated by marine algal organic matter and oxygen-depleted bottom waters (Beik et al., 2018, 2019; Giraldo-Gómez et al., 2018; Usman et al., 2025), while TOC, TON, and elemental geochemistry indicate enhanced productivity and fluctuating preservation conditions (Usman et al., 2025). A regional transect of seven wells documented the spatial and temporal transition from phosphatic facies to organic-rich deposits and overlying chalk facies (**Fig. 1**, Ardila-Sanchez et al., 2026 accepted). To investigate the drivers of environmental variability along the southern Tethyan margin during the Maastrichtian, we integrate high-resolution records of calcareous nannofossil and dinoflagellate cyst assemblages, siliceous microorganism abundances, stable isotopes ($\delta^{18}O$, $\delta^{13}C\_carb$, $\delta^{13}C\_org$, and $\delta^{15}N$), total organic carbon (TOC), C/N ratios, elemental geochemistry, and gamma-ray (GR) data from two continuously cored successions exceeding 200 m in thickness. This multiproxy dataset is used to reconstruct changes in productivity, bottom-water oxygenation, and organic-matter preservation across the transition from phosphatic to organic-rich and chalk facies. Particular emphasis is placed

https://doi.org/10.5194/egusphere-2026-3135
Preprint. Discussion started: 7 July 2026

on identifying the drivers of the pronounced TOC cyclicity and evaluating its relationship to orbital-scale insolation forcing, variability in upwelling intensity, and changes in organic-matter preservation. Furthermore, we assess how the Maastrichtian upwelling system responded to the Mid-Maastrichtian Event (MME), providing new insights into the sensitivity of greenhouse-climate upwelling systems to both orbital forcing and transient global warming.

2. Geological settings

During the Late Cretaceous, Jordan occupied the northwestern margin of the Arabian Plate along the southern Neo-Tethys Ocean, where shallow-marine carbonate sedimentation developed under greenhouse conditions and elevated eustatic sea levels (**Fig. 1a**) (Kalifi et al., 2025; Powell & Moh', 2011). Regional tectonic reorganization linked to the progressive closure of the Neo-Tethys induced both compressional deformation associated with the Syrian Arc system and extensional to transtensional tectonics within intraplate basins (Kalifi et al., 2025; Powell & Moh', 2011). In Jordan, this tectonic phase reactivated the NW–SE-trending Azraq–Hamza graben system, which reached peak activity during the early Campanian, followed by Maastrichtian–Eocene thermal subsidence that controlled accommodation space and sediment distribution (Kalifi et al., 2025). The Upper Cretaceous succession comprises the Ajlun and Belqa groups. The Ajlun Group records Late Albian–Coniacian, whereas the overlying Belqa Group spans the late Coniacian to Eocene and includes, in ascending order, the Wadi Umm Ghudran, Amman Silicified Limestone, Al Hisa Phosphorite, Muwaqqar Chalk Marl (MCM), Umm Rijam Chert, and Wadi Shallalah Chalk formations (Kalifi et al., 2025; Messaoud et al., 2025; Powell & Moh', 2011).

https://doi.org/10.5194/egusphere-2026-3135
Preprint. Discussion started: 7 July 2026

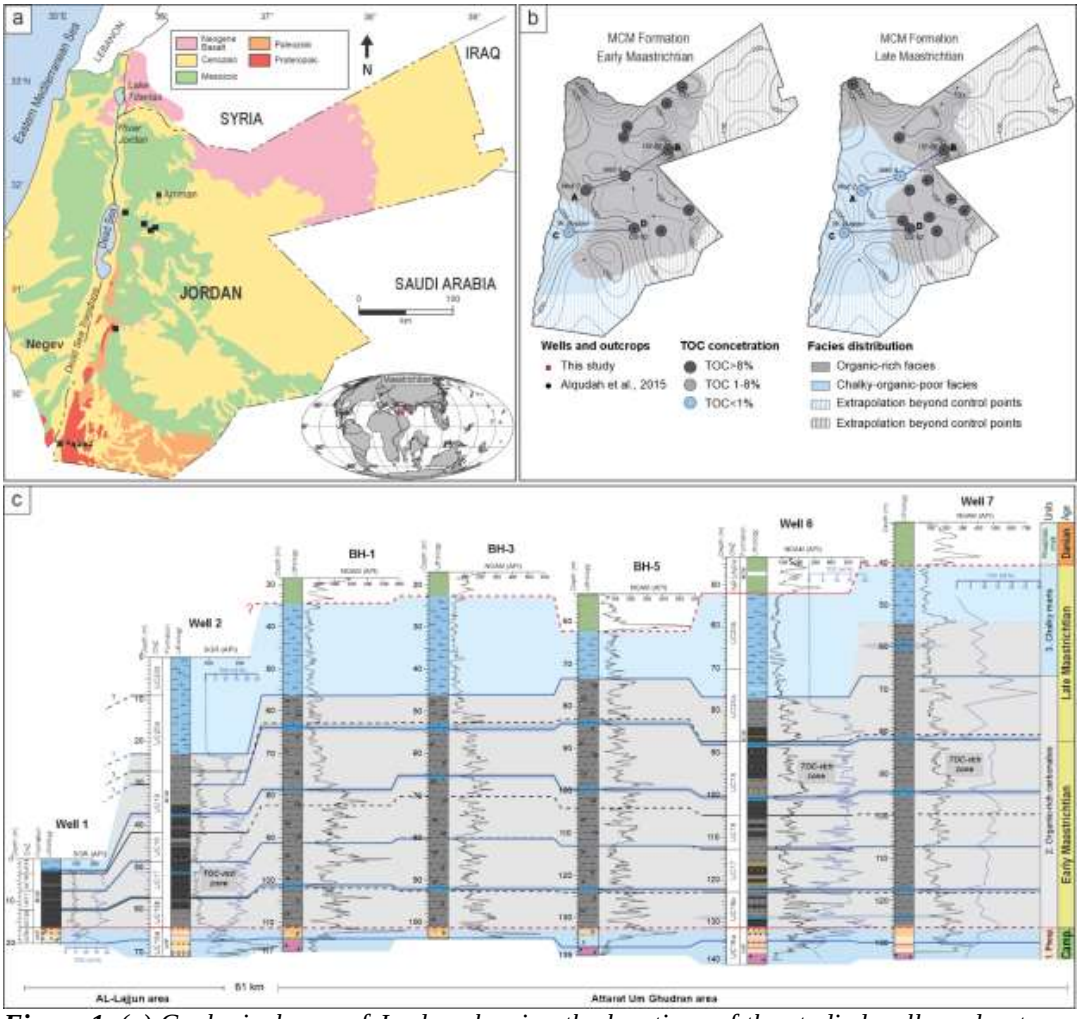

Figure 1. *(a) Geological map of Jordan showing the locations of the studied wells and outcrop (modified from Kalifi et al., 2025). (b) Isopach maps illustrating the spatial distribution of organic-rich facies within the Maastrichtian Muwaqqar Chalk Marl (MCM) Formation (after Kalifi et al., 2025). Calcareous nannofossil zonation and biostratigraphic data are compiled from Messaoud et al. (2025), (Alqudah et al., 2023), and (Beik et al., 2019). (c) Regional lithostratigraphic correlation of Maastrichtian sections in central Jordan, flattened at the base of UC16b corresponding to a major gamma-ray peak and phosphorite-rich horizon. Biostratigraphic and mineralogical data are from (Ardila-Sanchez et al., 2026 accepted)*

During the Santonian–Maastrichtian, the southern Neo-Tethyan margin was influenced by a persistent upwelling system that enhanced marine productivity and phosphogenesis (Almogi-Labin et al., 1993; Ashckenazi, 2012; Edelman-Furstenberg, 2009b; Meilijson et al., 2014). This

https://doi.org/10.5194/egusphere-2026-3135
Preprint. Discussion started: 7 July 2026

circulation system was likely driven by the combined effects of post-Santonian cooling, high sea levels, and plate reorganization along the southern Tethyan margin. The MCM Formation, the focus of this study, was deposited during a major Early Maastrichtian transgression across the Jordanian Plateau (Powell and Moh'd, 2011). It mainly consists of organic-rich chalks and marls interbedded with phosphatic limestones and chert horizons deposited under highly productive marine conditions linked to coastal upwelling (Giraldo-Gómez et al., 2018). TOC values commonly range between 3 and 30 wt.%, with organic matter dominated by Type II–IIS kerogen and sulfur contents between 2 and 12 wt.% (Abu-Mahfouz et al., 2022; Usman et al., 2025). Phosphatic and bituminous facies characterize the lower MCM, whereas the upper part becomes progressively more chalky and bioturbated, reflecting improved bottom-water oxygenation before deposition of the Umm Rijam Chert Formation (**Fig. 1c**; Powell and Moh'd, 2011; Ardila-Sanchez et al., 2026). Figure 1b *(Ardila-Sanchez et al., 2026 accepted)* illustrates the spatial distribution of total organic carbon (TOC) concentrations and depositional facies within the Maastrichtian MCM Formation during the early and late Maastrichtian. Organic-rich facies dominate the basin, particularly during the early Maastrichtian, when high TOC values (>8%) indicate widespread organic matter accumulation under suboxic to anoxic conditions. During the late Maastrichtian, chalky organic-poor facies expanded, reflecting reduced productivity and improved bottom-water oxygenation, while high-TOC zones became more restricted and shifted toward more proximal areas in the East. In Figure 1c (Ardila-Sanchez et al., 2026 accepted) presents a west–east stratigraphic correlation of wells and boreholes across central Jordan, showing lithology, gamma-ray logs, TOC trends, and depositional units of the Maastrichtian–Danian succession. The correlation highlights the development of a regionally extensive TOC-rich interval within the early Maastrichtian organic-rich carbonate unit (Unit 2), followed by a transition to chalky, organic-

https://doi.org/10.5194/egusphere-2026-3135
Preprint. Discussion started: 7 July 2026

poor deposits (Unit 3) during the late Maastrichtian. The figure also demonstrates the diachronous distribution of maximum TOC accumulation, with organic-rich conditions persisting longer in more proximal settings before the establishment of more oxygenated depositional environments.

3. Methods and dataset

This study is based on two continuously cored wells from central Jordan that cover the Maastrichtian interval of the Muwaqqar Chalk Marl (MCM) Formation. The SA-01 well, located in the Attarat Um Ghudran area, was selected as the reference section because it preserves a relatively complete Maastrichtian succession, including both organic-poor and organic-rich facies of the MCM Formation. The investigated interval is approximately 140 m thick and was described at a centimeter scale for lithology, texture, fabric, grain types, and sedimentary structures by Ardila-Sanchez et al. (2026). The AJ-02 well, drilled in the Al-Lajjun area, comprises a 75 m thick succession extending from the Campanian–Maastrichtian boundary to the Middle Maastrichtian and mainly targets the organic-rich oil shale interval of the MCM Formation. Usman et al. (2025) previously presented a detailed geochemical characterization of this core. In total, this study integrates observations from 215 m of well-preserved core material with recovery exceeding 90%. Slabbed cores were examined to identify lithofacies variations and to conduct geochemical analyses (Ardila-Sanchez et al., 2026; Usman et al., 2025). In addition, open-hole wireline logs, including GR and lithology-derived logs, were used to support well correlations and refine stratigraphic interpretations (Ardila-Sanchez et al., 2026; Kalifi et al., 2025).

3.1. Calcareous nannofossils

Calcareous nannofossil analyses were conducted on oil shale core samples from Jordan, including 56 samples from the AJ-02 core and 62 samples from the SA-01 core. Smear slides were prepared following standard procedures described by (Bown & Young, 1998). Small amounts of

https://doi.org/10.5194/egusphere-2026-3135
Preprint. Discussion started: 7 July 2026

sediment were dispersed in buffered deionized water (pH ~8.5) with the addition of a surfactant to enhance particle dispersion. After brief settling to eliminate coarse particles, the supernatant was transferred onto cover slips, dried at low temperature, and mounted onto glass slides using Norland optical adhesive (RI = 1.56) before ultraviolet curing. To minimize contamination, the external surfaces of the core samples were removed prior to preparation. Slides were examined under transmitted light microscopy at 1000× magnification using both plane-polarized and cross-polarized light following standard nannofossil procedures. References for calcareous nannofossils include (Perch-Nielsen, 1985) and (Bown & Young, 1998). The Cretaceous biozonation used here follows the CC scheme developed by (Sissingh, 1977), modified by Perch-Nielsen (1985), and the UC^{TP} (Tethyan Province) proposed by (Burnett, 1998) and (Thibault, 2016). We used the "NP" biozonation scheme of (Martini, 1971) for the Danian. Taxonomic concepts adhere to those outlined in Perch-Nielsen (1985) and Bown (1998). The zonation scheme in this study is based on Last Occurrence (LO) and First Occurrence (FO). In selected cases, scanning electron microscopy (SEM) was employed to verify the identification of small or poorly preserved taxa. Taxonomic identification and age assignments followed established Upper Cretaceous calcareous nannofossil biostratigraphic schemes, with particular emphasis on biostratigraphically and paleoecologically important species. Quantitative analyses were carried out by counting a minimum of 300 specimens per sample. Relative abundances were calculated as percentages of the total assemblage, while total abundance was estimated as the number of specimens per field of view (N/FOV). To simplify abundance analyses, species were grouped at the genus level (Razmjooei et al., 2020). The *Watznaueria* group includes *W. barnesiae*, *W. biporta*, and *W. ovata*; the *Retecapsa* group includes *R. angustiforata*, *R. crenulata*, and *R. ficula*; the *Micula* group includes *M. murus*, *M. praemurus*, *M. prinsii*, *M. cf. M. swastica*, and *Micula* sp. The *Zeugrhabdotus* group comprises

https://doi.org/10.5194/egusphere-2026-3135
Preprint. Discussion started: 7 July 2026

Z. bicrescenticus, *Z. embergeri*, *Zeugrhabdotus* sp., and *Placozygus fibuliformis*; the *Ceratolithoides* group includes *C. aculeus*, *C. indiensis*, *C. kamptneri*, *C. amplector*, *C. verbeekii*, and *Ceratolithoides* sp.; and the *Arkhangelskiella* group includes all morphotypes of *Arkhangelskiella cymbiformis*. *Cribrosphaerella ehrenbergii* and *Arkhangelskiella cymbiformis* were used as indicators of cooler surface-water conditions. *C. ehrenbergii* is a cosmopolitan species whose paleoecological affinity remains debated; however, several studies have associated its increased abundance with cooler water masses (Ovechkina & Alekseev, 2005; Watkins, 1992; Wise, 1983). Similarly, *A. cymbiformis* is widely distributed in Late Cretaceous marine settings but generally reaches its highest abundances at mid-latitudes and is commonly regarded as a cool-water taxon (Lees et al., 2005; Thibault & Gardin, 2006a; Thierstein, 1981). Consequently, fluctuations in the abundance of these two species were used in this study to infer relative variations in sea-surface temperature and to identify intervals characterized by cooler paleoceanographic conditions (Razmjooei et al., 2020).

3.2. Dinoflagellate cyst assemblages

Palynological analysis was conducted on 20 samples from the study interval to investigate marine organic-walled microfossils. Approximately 30 g of sediment per sample was processed at Global GeoLab Ltd. (Canada) using standard palynological preparation techniques, including HCl (38%) and HF (40%) acid digestion, heavy liquid separation ($ZnCl_2$ + HCl, density ~2.0 g/cm³), and sieving through a 15 µm mesh. Dinoflagellate cyst productivity varied across the dataset: some samples were barren, others were sparsely to moderately productive, while several yielded highly productive assemblages suitable for quantitative analysis (typically >200 cysts per sample), allowing reliable relative abundance calculations. Relative abundance classes follow Pospelova et al. (2004), ranging from present (>0–1%), rare (>1–5%), common (>5–30%), abundant (>30–

https://doi.org/10.5194/egusphere-2026-3135
Preprint. Discussion started: 7 July 2026

50%), to dominant (>50%). Palynological slides were examined under a Zeiss Axioscope microscope, and all residues and slides are archived in the institutional collection.

3.3. Stable isotopes analysis

For organic carbon and nitrogen analyses, 1–2 g of dried and ground rock powder was decarbonated using 2 M HCl to remove the carbonate fraction. Samples were thoroughly mixed using a vortex shaker to ensure complete reaction, followed by repeated rinsing with double-distilled water until the absence of chloride ions was confirmed with silver nitrate. The treated residues were then used for measurements of total carbon (wt% C) and nitrogen (wt% N) as well as their isotopic compositions. Total organic carbon (TOC) and total organic nitrogen (TON) were calculated from the measured C and N values after correcting for the removed $CaCO_3$ fraction. Carbon and nitrogen isotopes were measured simultaneously from the same sample by peak jumping, with analytical precision of ±0.19‰ for $\delta^{13}C_{org}$ and ±0.28‰ for $\delta^{15}N_{org}$. Isotopic values are reported relative to PDB for carbon and atmospheric air for nitrogen. An internal lignin standard was run every 6–8 samples to monitor analytical stability and prevent instrumental drift.

4. Results

4.1. Cores description

4.1.1. AJ-02 core

The AJ-02 core consists for the upper part of 24m of cuttings and for the lower part of 47m of well preserved core (**Fig. 2**). The downhole spectral gamma ray (SGR) profile generally follows the uranium (U) concentration profile, whereas thorium (Th) and potassium (K) show limited variation. The highest SGR values occur between 63 and 72 m depth within the AHP interval. Above this, the organic matter-rich chalk interval extends from 21 to 63 m and displays SGR

https://doi.org/10.5194/egusphere-2026-3135
Preprint. Discussion started: 7 July 2026

values ranging from 20 to 90 counts. The organic matter-rich chalk interval (24–63 m; ~39 m thick) contains TOC values ranging from 2 to 22 wt% with an average of 14 wt%. The AHP interval (63–71 m; ~8 m thick) contains TOC values ranging from 0.1 to 14 wt% with an average of 6 wt%. Three geochemical cycles were identified by Usman et al. (2025) within the organic matter-rich chalk interval. Cycle 1 extends from 49 to 62.5 m depth (~13.5 m thick) and contains TOC values ranging from 10.55 to 22.19 wt% and total sulfur (TS) values ranging from 2.74 to 4.95 wt%. Cycle 2 extends from 37 to 49 m depth (~12 m thick) and contains TOC values ranging from 6.32 to 19.92 wt% and TS values ranging from 1.67 to 4.98 wt%. Cycle 3 extends from 24 to 37 m depth (~13 m thick) and contains TOC values ranging from 2.38 to 17.32 wt% and TS values ranging from 0.67 to 4.35 wt%. The modified van Krevelen diagram classifies the organic matter as mixed Type I–II kerogen (Usman et al., 2025), while sulfur index values classify the kerogen as Type IIS. XRD analysis shows that the mineralogical composition is dominated by carbonate minerals, mainly calcite, ranging from 20 to 80%, with occasional dolomite (Usman et al., 2025). Silicate minerals range from 5 to 20%, with localized values reaching up to 56%. Clay minerals range from 1 to 6%, with kaolinite as the dominant clay mineral. Fluorapatite ranges from 2 to 12%, gypsum from 1 to 10%, pyrite from 1 to 10%, and sphalerite from 1 to 5%.

Cycles 1 and 3 are characterized by carbonate contents averaging approximately 70%, silicate contents ranging from 10 to 20%, and clay contents below 5%. At 58.5 m depth, quartz and clay contents increase while calcite decreases. Cycle 2 contains silicate contents ranging from 6 to 56%, carbonate contents ranging from 20 to 60%, and clay contents below 4%. Opal CT occurs mainly within Cycle 2. XRF data show high CaO concentrations throughout the section, with variable Al2O3 and SiO2 contents. Elevated SiO2 values occur within Cycle 2. P2O5 concentrations reach up to 10%, with higher values in the AHP interval. Trace-element data show

https://doi.org/10.5194/egusphere-2026-3135
Preprint. Discussion started: 7 July 2026

enrichments in P, Zn, Cr, Mo, U, Cd, Ni, Cu, and V (Usman et al., 2025). Al contents within the organic matter-rich chalk interval range from 2 to 8%, with higher values occurring at the top and bottom of the section.

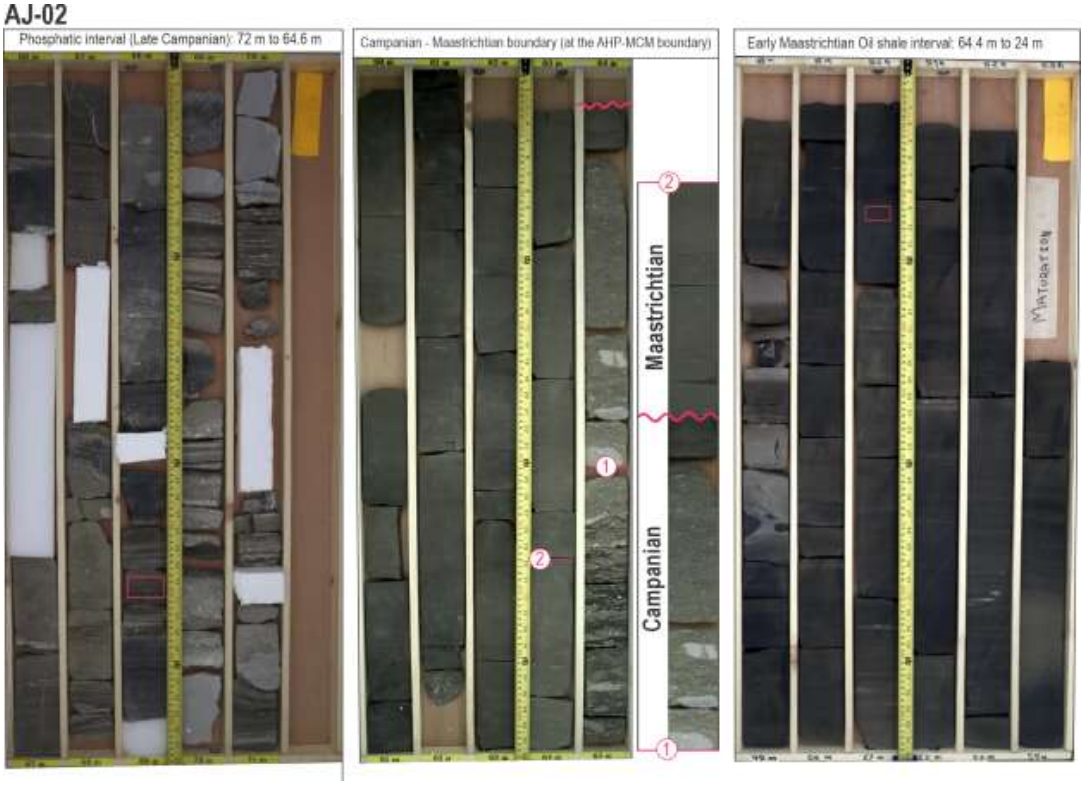

Figure 2. *Representative core photographs and petrographic images from the AJ-02 core illustrating the lithological variability across the Campanian–Maastrichtian succession and the transition between the AHP and MCM formations. The left panel shows the phosphatic interval of the Campanian succession characterized by dark phosphatic and organic-rich lithologies. The central panel highlights the Campanian–Maastrichtian boundary at the contact between the AHP and MCM formations, marked by a transition from phosphatic deposits to organic-rich marls. Thin-section photomicrographs on the right show representative microfacies, including organic-rich fine-grained carbonate mudstones and phosphatic peloidal facies with abundant phosphatic grains and bioclasts. Red boxes indicate the location of sampled intervals, while red wavy lines mark major stratigraphic boundaries.*

https://doi.org/10.5194/egusphere-2026-3135
Preprint. Discussion started: 7 July 2026

4.1.2. SA-01 core

The SA-01 core was fully recovered and comprises four main lithostratigraphic units spanning the uppermost AHP Formation and the MCM Formation (**Fig. 3**). The basal interval (139.45–131.8 m) consists of a phosphorite-rich unit characterized by upward-coarsening phosphatic marls and bioturbated phosphorites with moderate to high organic matter content and elevated phosphate concentrations, locally reaching 14.1 wt.% P_2O_5. This interval also contains carbonate and chert concretions together with siliceous mudstones, and its upper boundary marks the transition between the AHP and MCM formations. Organic-rich carbonate sediments composed mainly of bituminous marls and chalky marls with high $CaCO_3$ and TOC values dominate overlying this interval, the lower MCM Formation (131.8–76.95 m). Lithologies range from strongly bioturbated to laminated facies, include several dolomitic beds, and lag deposits. The middle MCM interval (76.95–52 m) consists predominantly of light-colored chalky marls and carbonate-rich sediments, represented mainly by foraminiferal packstones and planktonic foraminiferal mudstone–wackestones with coccolith-rich matrices. Toward the upper part of this interval, carbonate content decreases slightly while reddish beds and increased siliciclastic input become more prominent, marking the interpreted K/Pg boundary. The uppermost part of the core (9 m, upper MCM Formation) is composed of phosphatic chalks rich in carbonate and locally enriched in silica due to chalcedony precipitation within foraminiferal tests. The succession grades upward from reddish marly chalks into bioturbated phosphatic chalks and peloidal-rich facies associated with elevated phosphate concentrations and high gamma-ray values.

https://doi.org/10.5194/egusphere-2026-3135
Preprint. Discussion started: 7 July 2026

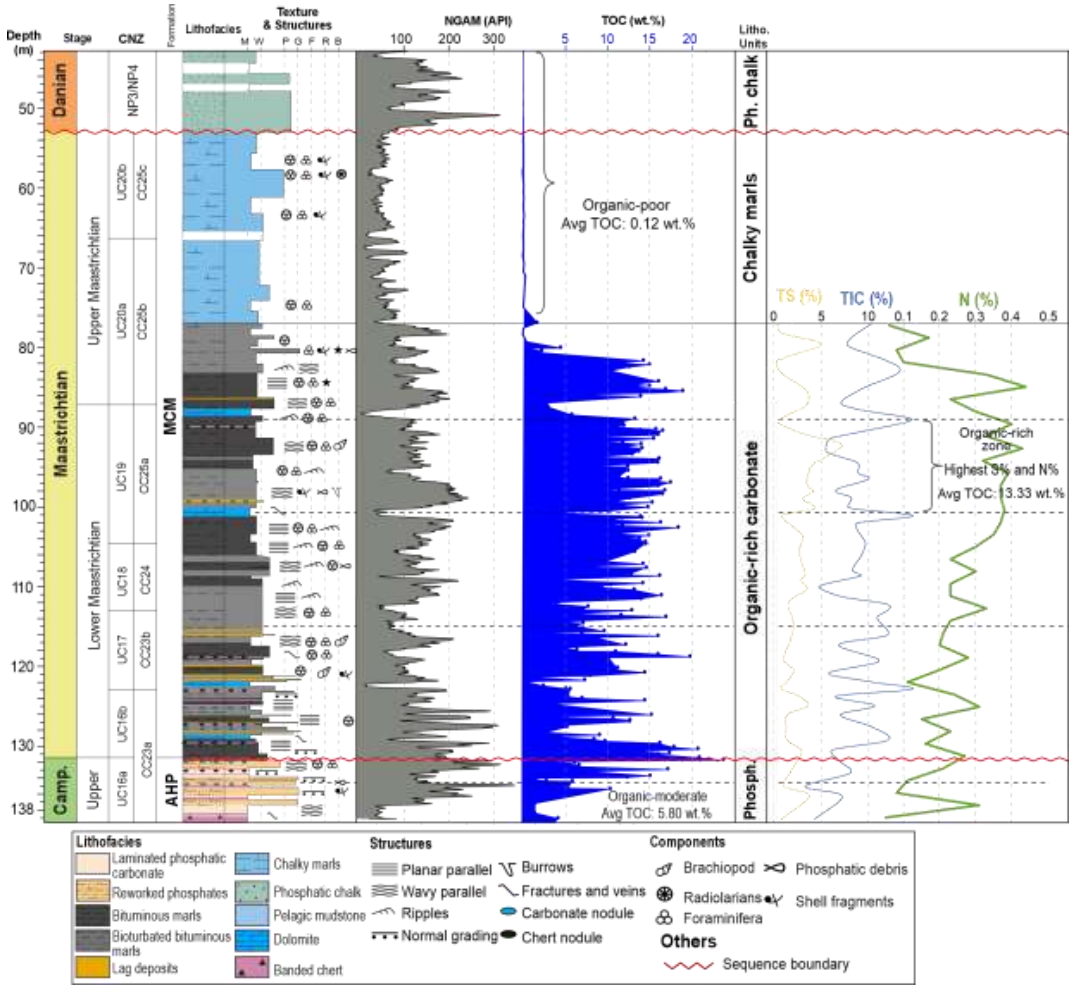

Figure 3. *Lithostratigraphic log and geochemical profile of the SA-01 core across the upper Campanian–Maastrichtian to lower Danian succession, showing the transition from the phosphatic interval of the AHP Formation into the organic-rich carbonate succession of the MCM Formation. The figure illustrates the distribution of lithofacies, sedimentary structures, and major fossil components together with gamma-ray response and selected geochemical parameters, including TOC, TS, total inorganic carbon (TIC), and nitrogen (N). The lower part of the succession is dominated by phosphatic carbonates, reworked phosphates, bituminous marls, and laminated phosphatic facies, followed upward by organic-rich marls and chalky marls of Maastrichtian age. The upper interval consists mainly of chalky marls, phosphatic chalks, and pelagic mudstones deposited across the Maastrichtian–Danian transition. Red wavy lines indicate major stratigraphic boundaries, including the inferred K/Pg boundary.*

https://doi.org/10.5194/egusphere-2026-3135
Preprint. Discussion started: 7 July 2026

4.2. Calcareous nannofossils

4.2.1. Aj-02 core

The studied succession yielded moderately preserved calcareous nannofossil assemblages of Maastrichtian age, composed mainly of marine coccoliths and nannoliths. The most common taxa include *Watznaueria* spp., *Ceratolithoides ehrenbergii*, *Retecapsa* spp., *Micula* spp., *Eiffellithus* spp., *Tranolithus* spp., and *Arkhangelskiella* spp. (**Fig. 4**). Calcareous nannofossil assemblages are strongly dominated by Watznaueria spp. Its relative abundance remains generally below 30% between 67 and 24.2 m depth, fluctuating around 20–30% of the assemblage. Above 24.2 m, *Watznaueria* spp., shows a marked increase, exceeding 50% of the assemblage between 24.2 and 4 m, where it becomes overwhelmingly dominant and reaches its highest values in the uppermost part of the section. *C. ehrenbergii* is the second most abundant taxon in the lower part of the section. Its abundance is relatively high between 67 and 24.2 m, commonly ranging between 5 and 15%, with local maxima around 30–35 m depth. Up-section, its abundance progressively decreases and remains low above 24.2 m. *Retecapsa* spp. display moderate abundances throughout the section, generally ranging between 5 and 15%. The genus is relatively common in the 67–24.2 m interval, with several peaks in the middle part of the section, but shows a gradual decline toward the upper Maastrichtian. *Micula* spp. occur continuously but in lower proportions than Watznaueria. Their abundance is relatively stable in the lower interval (67–24.2 m), generally between 5 and 10%, and decreases slightly upward, although minor fluctuations are observed in the upper part of the section. *Eiffellithus* spp. and Tranolithus spp. are consistently present but remain subordinate components of the assemblage. Both genera show moderate abundances in the lower Maastrichtian interval and tend to decrease upward, particularly above 24.2 m, where they constitute only a minor fraction of the nannofossil community. *Arkhangelskiella* spp. occur

https://doi.org/10.5194/egusphere-2026-3135
Preprint. Discussion started: 7 July 2026

throughout the section with relatively low to moderate abundances. Their distribution broadly follows the trend observed for *Retecapsa* and *Micula*, with slightly higher values in the lower and middle parts of the section and lower abundances toward the top. .

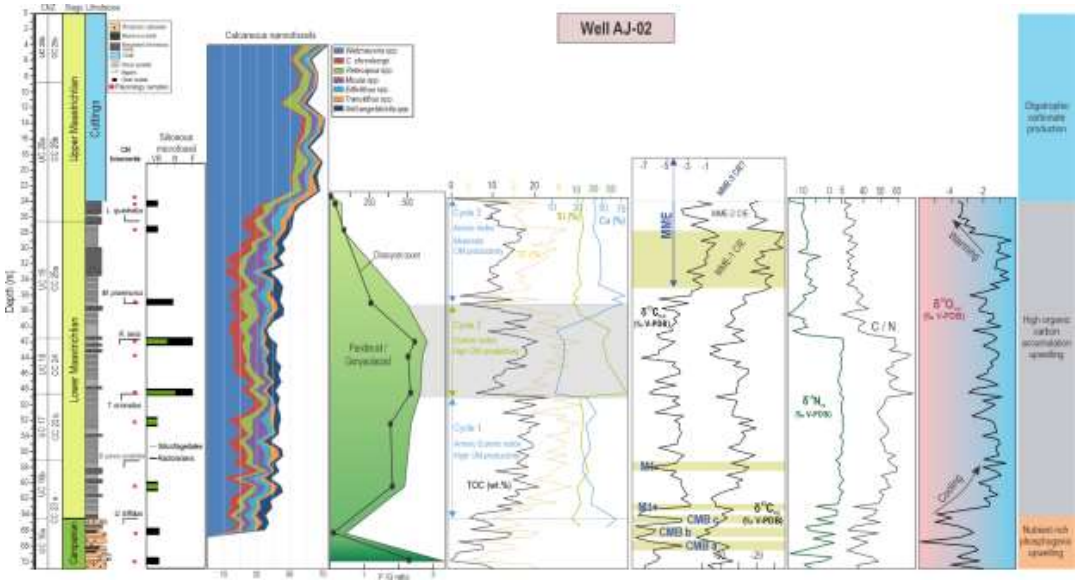

Figure 4. *Integrated stratigraphic, micropaleontological, geochemical, and paleoenvironmental interpretation of the AJ-02 core spanning the upper Campanian to upper Maastrichtian succession. The figure combines lithostratigraphy, calcareous nannofossil assemblage variations, dinoflagellate cyst distribution, organic geochemical proxies, stable isotope records, and sequence stratigraphic interpretation. The left panel shows the lithological succession and calcareous nannofossil relative abundances through the UC and CC biozones, together with the occurrence of selected dinocyst taxa and siliceous microfossils. Variations in TOC, TS, Si, and Ca contents are used to define three depositional cycles characterized by fluctuating productivity and redox conditions, ranging from anoxic–euxinic to more oxygenated environments. The middle panels illustrate sequence stratigraphic interpretation, including maximum flooding surfaces (MFS), transgressive surfaces, and condensed phosphatic intervals associated with phosphogenesis and enhanced organic matter preservation. Carbon and oxygen isotope trends, together with C/N ratios, indicate changes in paleoproductivity, nutrient supply, and cooling conditions through the Maastrichtian. The right panel summarizes the interpreted paleoenvironmental evolution from nutrient-rich phosphogenic upwelling conditions during the Campanian to enhanced organic carbon accumulation and oligotrophic carbonate production during the Maastrichtian.*

https://doi.org/10.5194/egusphere-2026-3135
Preprint. Discussion started: 7 July 2026

4.2.2. SA-01 core

The *Watznaueria* spp. curve is the most dominant throughout the studied interval, exhibiting consistently high percentages ranging approximately between 20% and 45%. The genus shows a gradual increase from the Campanian upward into the Maastrichtian, reaching its highest abundance within the middle Maastrichtian interval before slightly decreasing near the K/Pg boundary. This persistent dominance indicates stable open-marine conditions and warm surface-water environments during deposition.

The *Prediscosphaera* spp. curve displays moderate but fluctuating abundances, generally varying between 2% and 15%. The genus is relatively scarce in the lower Campanian interval but becomes more common upward through the Maastrichtian, where several short abundance peaks are recorded. Its decline close to the K/Pg boundary suggests increasing paleoenvironmental stress during the latest Maastrichtian. The *Micula* spp. curve shows a pronounced upward increase throughout the Maastrichtian succession.

https://doi.org/10.5194/egusphere-2026-3135
Preprint. Discussion started: 7 July 2026

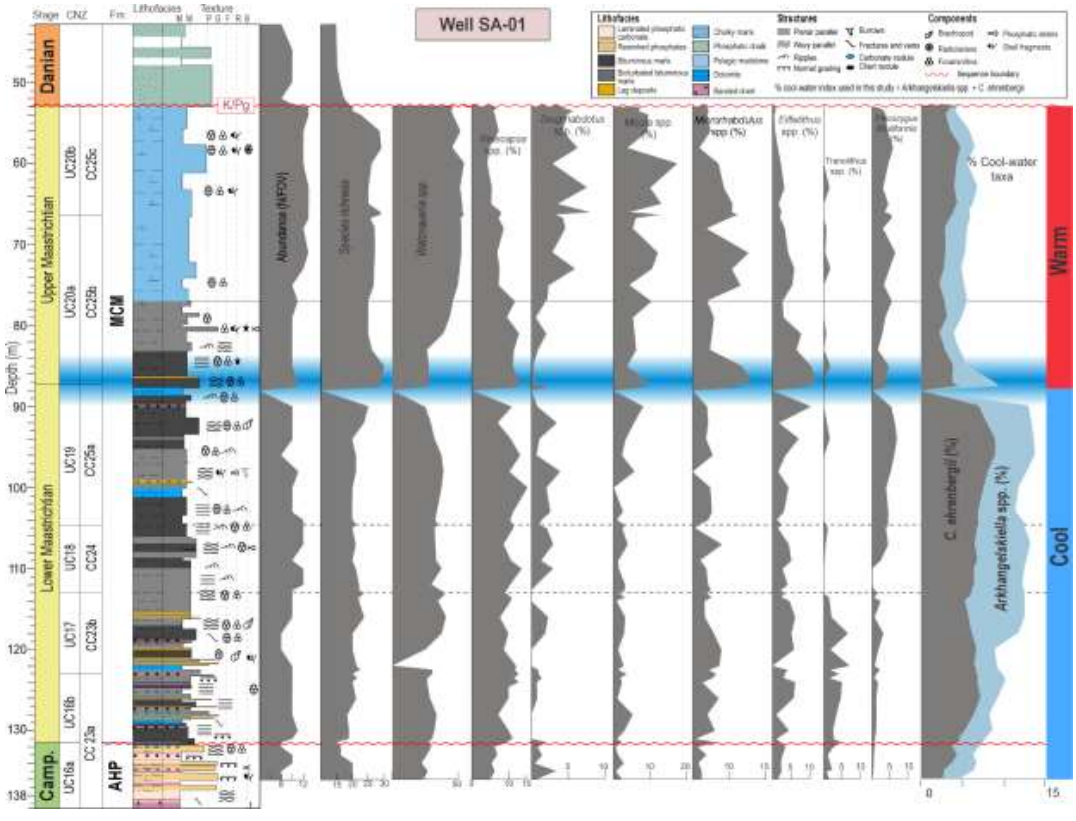

364

https://doi.org/10.5194/egusphere-2026-3135
Preprint. Discussion started: 7 July 2026

Figure 5. *Integrated lithostratigraphic, biostratigraphic, and paleoecological framework of the SA-01 core spanning the upper Campanian to lower Danian succession. The figure shows the distribution of lithofacies, sedimentary structures, and fossil components together with calcareous nannofossil abundance and relative abundance patterns of selected taxa across the UC and CC biozones. The succession records the transition from phosphatic deposits of the AHP Formation into the carbonate-rich sediments of the MCM Formation. Variations in total nannofossil abundance (N/FOV) and species richness are illustrated alongside the distribution of key Maastrichtian taxa, including Watznaueria spp., Retecapsa spp., Zeugrhabdotus spp., Micula spp.,* Microrhabdulus *spp.,* Eiffellithus *spp.,* Tranolithus *spp., and* Placozygus fibuliformis. *The lower Maastrichtian interval is characterized by increased abundance of cool-water taxa, particularly* Arkhangelskiella *spp. and* Cribrosphaerella ehrenbergii, *indicating cooler and more nutrient-rich surface-water conditions. Up-section, assemblages shift toward warmer-water taxa and reduced cool-water indicators during the late Maastrichtian and early Danian. Red wavy lines denote major stratigraphic boundaries, including the Campanian–Maastrichtian transition and the inferred K/Pg boundary.*

Abundances are very low in the Campanian section, commonly below 5%, but progressively rise upward to values exceeding 15–20% within the upper Maastrichtian. This marked increase reflects the growing importance of *Micula* taxa during the latest Cretaceous and supports a Maastrichtian age assignment for the studied interval. The curve decreases abruptly across the K/Pg boundary. The *Microrhabdulus* spp. curve remains generally low and irregular throughout the section, mostly fluctuating between 1% and 8%. Slight increases are observed within the middle Maastrichtian interval; however, the group never becomes dominant.

The *Eiffellithus* spp. curve is characterized by sporadic occurrences and low percentages, generally ranging between 1% and 6%, with occasional minor peaks. Preservation features such as overgrowth and dissolution are evident in several intervals, which likely affected the abundance distribution of this taxon. The genus becomes increasingly rare upward toward the upper Maastrichtian and nearly disappears across the K/Pg transition.

The *Tranolithus* spp. curve exhibits consistently low abundances throughout the entire section, rarely exceeding 5%. The taxon occurs intermittently and does not show any major stratigraphic expansion, indicating a limited ecological contribution to the assemblage composition.

https://doi.org/10.5194/egusphere-2026-3135
Preprint. Discussion started: 7 July 2026

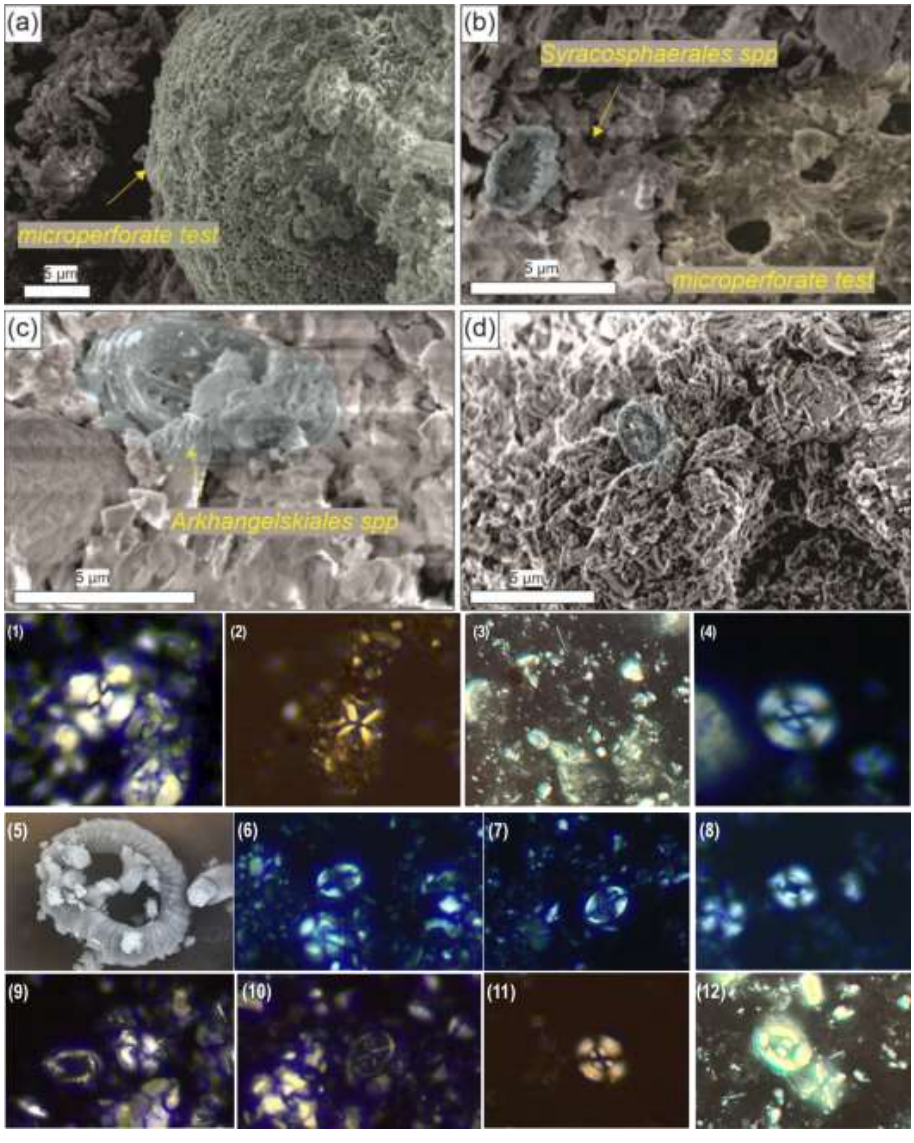

Figure 6. *Representative scanning electron microscope (SEM) and light microscope images of selected calcareous nannofossils and associated microfossils identified in the Maastrichtian succession of the studied cores. SEM images (a–d) illustrate examples of microperforate tests and associated coccolith taxa, including Syracosphaerales spp. and Arkhangelskiella spp., preserved within carbonate-rich matrices. Light microscope photomicrographs under crossed-polarized and plane-polarized light (1–12). 1) and 4) Watznaueria barnesae. 2) Micula staurophora. 3) Rhagodiscus angustus. 5) Watznaueria biporta. 6) and 7) Eiffellithus eximius. 8) and 11) Watznaueria ovata. 9) Cribrosphaerella ehrenbergii. 10) Chiastozygus synquadriperforatus. 12) Zeugrhabdotus embergeri.*

https://doi.org/10.5194/egusphere-2026-3135
Preprint. Discussion started: 7 July 2026

The *Kamptnerius magnificus* curve also shows very low and discontinuous occurrences, generally below 3–4%. The species appears sporadically within the Maastrichtian interval and may reflect localized environmental conditions or preservational effects. The paleoclimatic curves (**Fig. 5**) reveal a gradual transition from relatively cool-water assemblages in the lower part of the section toward warmer-water assemblages upward into the upper Maastrichtian and Danian. Cool-water taxa, particularly *Arkhangelskiella* spp. and *Cribrosphaerella ehrenbergii*, are more common within the UC17 to UC19 intervals but decline in the upper UC19 zone and remain low, below 5%, through UC20a and UC20b zones (**Fig. 5**). In contrast, warm-water taxa increase markedly within the upper Maastrichtian, coinciding with the expansion of *Watznaueria*, *Micula*, and *Prediscosphaera*. This upward warming trend strats at the upper part of UC19 zone in both cores (Figs. 4 and 5).

4.3. Dinoflagellate cyst

Of the eleven samples, only one was found to be barren of dinoflagellate cysts, while 4 were sparsely to moderately productive, and seven were highly productive, yielding statistically significant sample sizes (counts >200 cysts) enabling robust relative abundance calculations (see dataset). Terminology relating to classes of relative abundance follows the parameters of Pospelova et al. (2004): present (>0 1%); rare (>1 5%); common (>5 30%); abundant (>30 50%); dominant (>50%). The material was generally well preserved. Overall, dinoflagellate cyst diversity was somewhat low, with at least thirty-one species belonging to nineteen genera having been identified. However, approximately half of the species observed were peridinioid taxa belonging to the genera *Alterbidinium*, *Andalusiella*, *Cerodinium*, *Isabelidinium*, *Lejeunecysta*, *Palaeocystodinium*, *Phelodinium*, *Senegalinium*, and *Vozzhennikovia*.

https://doi.org/10.5194/egusphere-2026-3135
Preprint. Discussion started: 7 July 2026

At 70.0 m, the assemblage includes dinoflagellate cysts such as *Cerodinium cf. albertii*, *Cerodinium cf. navarranium*, *Cerodinium striatum*, and *Hafniasphaera* spp., together with *Lejeunecysta* sp., *Palaeocystodinium golzowense*, and rare *Spiniferites* spp. Additional marine components include *Pterospermopsis* spp. and serial foraminiferal linings. Taxonomic remarks note open nomenclature for *Cerodinium cf. albertii* and *C. cf. navarranium* due to morphological variability and limited specimen counts (Corradini, 1973; Srivastava, 1995). The assemblage is dominated by marine palynomorphs (~35% minerals, ~30% AOM, ~30% dinoflagellate cysts, ~5% phytoclasts), with peridinioid taxa (*C. navarranium*) making up >98% of dinocysts, indicating high productivity conditions. Age interpretation of sample at 70 m level indicates Late Cretaceous (Early Maastrichtian–Late Maastrichtian). Stratigraphic ranges include: *Cerodinium cf. albertii* (Corradini, 1973), *C. navarranium* (Srivastava, 1995; Sweeney & Sullivan, 2004), and *C. striatum* with reported FO/LO ranges spanning ~67.3–56 Ma (various sources including Brinkhuis et al., 2003; Eshet et al., 1992; Powell, 1992; Köthe, 2012; Heilmann-Clausen, 1985; Bijl, 2022 DINOSTRAT supplement).

At 66.4 m, the assemblage is characterized by very high AOM (~95%) and minor phytoclasts (~5%), with isolated serial foraminiferal organic linings and trilete spores. *Spiniferites* spp. are present but extremely rare (only nine specimens), and no other dinoflagellate cysts or acritarchs were recorded. This indicates a strongly restricted marine environment with extremely high organic matter preservation and very low planktonic diversity.

At 60.5 m, the assemblage is dominated by organic matter (AOM ~80%) with subordinate phytoclasts (~24%) and minor foraminiferal organic linings (~1%). Terrestrial palynomorphs and trilete spores occur in low abundance. The sample is barren of dinoflagellate cysts and acritarchs.

https://doi.org/10.5194/egusphere-2026-3135
Preprint. Discussion started: 7 July 2026

Overall, the composition indicates a strongly organic-rich marine setting with limited terrestrial input, where preservation of AOM dominates the palynofacies signal.

At 52.4 m level (Core AJ-02, Well B; Pa05; Sample ID: AJ-02 R-4010-12/COR), the dinoflagellate cyst assemblage includes *Alterbidinium varium*, *Amphorosphaeridium fenestratum*, *Andalusiella mauthei*, *Dinogymnium acuminatum*, *Hafniasphaera* spp., *Isabelidinium cf. cooksoniae*, *Phelodinium gaditanum*, *Senegalinium macroocystum*, and *Spiniferites* spp. The assemblage is dominated by marine dinocysts with AOM (~40%), followed by phytoclasts (~25%) and dinocysts (~25%). *Alterbidinium varium* is the most abundant taxon (46.4%), while Spiniferacean taxa (*Spiniferites* spp. and *Hafniasphaera* spp.) together form ~48.2% of the assemblage. *Isabelidinium cf. cooksoniae* and *Senegalinium macroocystum* occur rarely (<1%), with other taxa present only as accessory components. Occasional terrestrial palynomorphs (saccate pollen, spores) are rare.

At the 48.5 m level, dinoflagellate cysts include *Andalusiella mauthei*, *Palaeocystodinium golzowense*, *Phelodinium gaditanum*, *Senegalinium* sp., and *Spiniferites* sp. The assemblage composition shows principal components of ~90% AOM and ~10% phytoclasts. Peridinioid dinoflagellate cysts dominate the assemblage, with *Andalusiella mauthei* (48.5%) and *Phelodinium gaditanum* (39.7%) being abundant, along with outlying specimens of *Senegalinium* sp. (7.4%) and *Palaeocystodinium golzowense* (1.5%). Beyond these taxa, only two specimens of non-peridinioid affinity were observed, identified as *Spiniferites* sp. Examples of marine acritarchs assignable to the genus *Fromea* are present but rare, along with the more frequent occurrence of serial foraminiferal organic linings. Age inference is Late Cretaceous (middle Santonian–late

https://doi.org/10.5194/egusphere-2026-3135
Preprint. Discussion started: 7 July 2026

Maastrichtian). For *Andalusiella mauthei*, the FO is 83.6 Ma (Masure et al. 1998, **Fig. 2**) and the LO is ~66.04 Ma (Masure et al. 1998).

At the 44 m level (AJ-02), the dinoflagellate cyst assemblage is dominated by *Andalusiella mauthei*, *Hafniasphaera* spp., *Hystrichosphaeridium tubiferum*, *Isabelidinium cretaceum*, *Spiniferites* spp., *Tanyosphaeridium xanthopyxides*, and *Vozzhennikovia* sp. The assemblage is characterized by approximately 90% amorphous organic matter (AOM) and 10% phytoclasts, while chorate acritarchs constitute 53% of the marine assemblage, excluding foraminiferal organic linings. The most abundant taxa are *Spiniferites* spp. (41.9%), *Vozzhennikovia* sp. (32.3%), *Tanyosphaeridium xanthopyxides* (9.7%), and *Isabelidinium cretaceum* (6.5%), whereas *Andalusiella mauthei*, *Hafniasphaera* spp., and *Hystrichosphaeridium tubiferum* each account for 3.2%. This association indicates a Late Cretaceous age, specifically middle Santonian to early Maastrichtian, consistent with the reported first and last occurrence data for *Andalusiella mauthei* and *Isabelidinium cretaceum* (Masure et al., 1998; Helby et al., 1987; Williams et al., 1993; Mohr & Mao, 1997; Piaszecki et al., 1992; Bijl, 2022; Thorn et al., 2009).

At the 41.9 m level in Core AJ-02, the assemblage is dominated by *Senegalinium macrocystum*, with subordinate *Andalusiella mauthei*, *Dinogymnium acuminatum*, *Hafniasphaera* spp., *Operculodinium?* sp., and *Spiniferites* spp. The assemblage comprises approximately 55% dinoflagellate cysts, 30% AOM, and 15% phytoclasts, with *S. macrocystum* accounting for 94.3% of the dinoflagellate cyst population. *Spiniferites* spp. account for 5.2%, whereas *Andalusiella mauthei*, *Dinogymnium acuminatum*, *Hafniasphaera* spp., and *Operculodinium* spp. are each present at less than 1%. The abundance of *S. macrocystum*, which occurs as thousands of cysts per slide, suggests a highly productive marine setting, and the assemblage also includes rare serial

https://doi.org/10.5194/egusphere-2026-3135
Preprint. Discussion started: 7 July 2026

foraminiferal organic linings, scolecodonts, and trilete spores. The age is interpreted as Late Cretaceous, specifically Late Campanian, consistent with the cited occurrence ranges for *Andalusiella mauthei* and *Dinogymnium acuminatum* (Masure et al., 1998; Olde et al., 2015; Lebedeva et al., 2013; Prince et al., 2008; McLachlan et al., 2018; Williams et al., 2004 sensu Fensome et al., 2008; Eshet et al., 1992; Bijl, 2022; Cookson & Eisenack, 1960).

At 37 m level, palynological analysis yielded a low-diversity dinoflagellate cyst assemblage dominated by peridinioid taxa. The assemblage is composed of approximately 90% amorphous organic matter (AOM) and 10% phytoclasts. Three dinoflagellate cyst taxa were identified: *Andalusiella gabonensis*, *Andalusiella mauthei*, and *Dinogymnium acuminatum*. *Andalusiella gabonensis* is the dominant species, comprising 74% of the assemblage (18 specimens), while *Andalusiella mauthei* accounts for 24% (6 specimens). Together, these taxa constitute approximately 98% of the total dinoflagellate cyst assemblage, indicating a highly productive depositional environment. A single specimen of *Dinogymnium acuminatum* was also observed.

At 27.6 m, the assemblage is dominated by *Senegalinium macrocystum*, with subordinate *Hafniasphaera* sp. and *Phelodinium gaditanum*. The sample is characterized by approximately 95% amorphous organic matter (AOM) and 5% phytoclasts, and palynomorphs are exceedingly rare, represented only by isolated specimens of *Hafniasphaera* sp., *Phelodinium gaditanum*, and *Senegalinium macrocystum*. At 24.3 m, the dinoflagellate cyst assemblage is extremely sparse and consists of *Spiniferites* sp. with very rare *Phelodinium gaditanum*, and *Vozzhennikovia?* sp. The sample is composed of approximately 95% AOM and 5% phytoclasts, whereas *Phelodinium gaditanum* and *Vozzhennikovia?* sp. are each represented by two specimens. Marine acritarchs

https://doi.org/10.5194/egusphere-2026-3135
Preprint. Discussion started: 7 July 2026

belonging to the genus *Fromea* are frequently observed, along with serial and biserial foraminiferal organic linings.

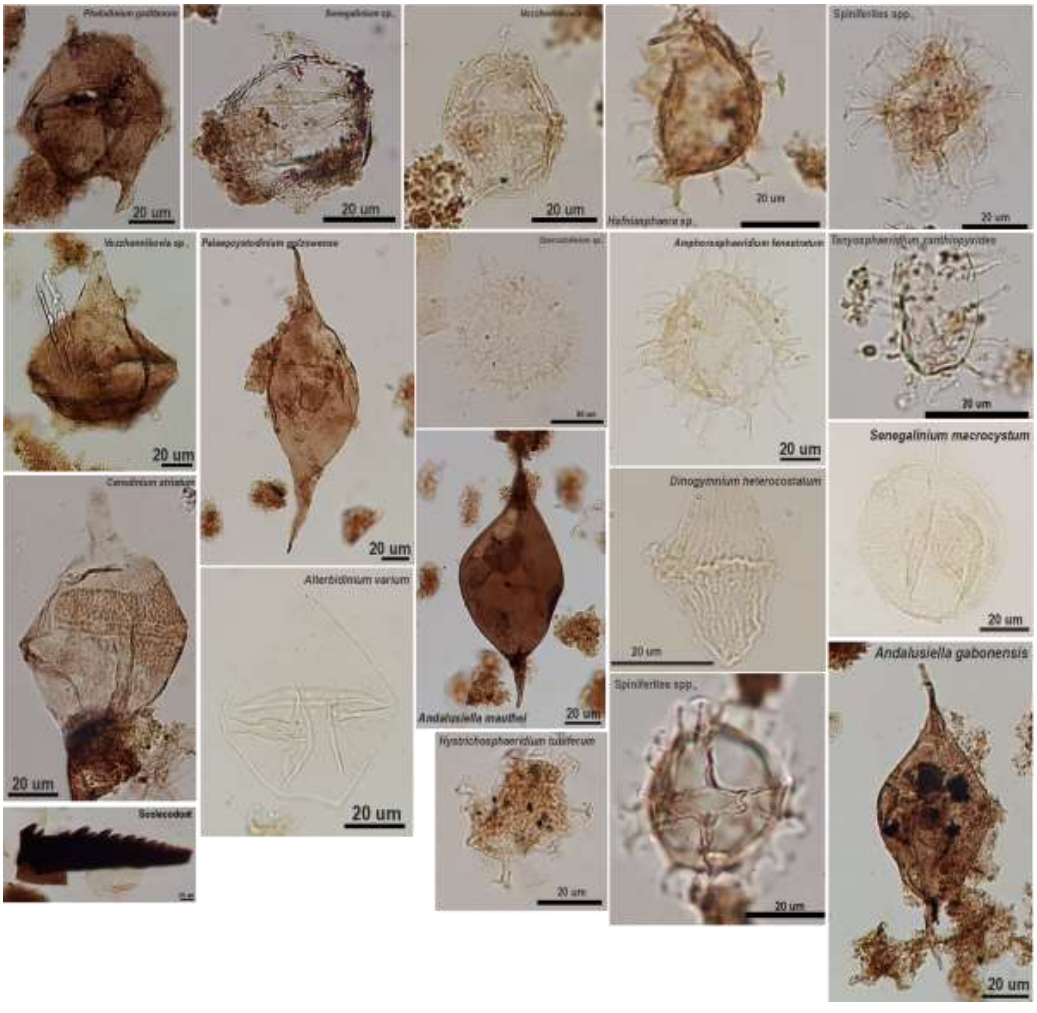

Figure 7. Representative dinoflagellate cysts and associated palynomorphs identified from the Maastrichtian succession of the studied cores. The assemblages are dominated by peridinioid and gonyaulacoid dinocysts, reflecting variations in marine productivity, nutrient availability, and paleoenvironmental conditions during deposition. A scolecodont fragment is also shown. Scale bars equal 20 µm.

https://doi.org/10.5194/egusphere-2026-3135
Preprint. Discussion started: 7 July 2026

4.4. $\delta^{13}C_{carb}$ and $\delta^{13}C_{org}$ isotope stratigraphy in AJ-02 core

The $^{13}C_{carb}$ and $\delta^{13}C_{org}$ isotope curves show significant fluctuations throughout the Campanian–Maastrichtian succession (**Fig. 4**). The interval between 71 and 64 m is characterized by depleted values, with $\delta^{13}C_{carb}$ ranging from −6‰ to −2‰ and δ^{13}Corg from −31‰ to −28.5‰. This pronounced negative excursion at the AHP–MCM transition is followed by a positive shift that marks the Campanian–Maastrichtian Boundary Event. Up-section, both curves display progressive ^{13}C enrichment through the Maastrichtian, indicating enhanced marine productivity and increased organic carbon burial. The interval between 37 and 29 m records a distinct positive excursion, where $\delta^{13}C_{org}$ values rise to about −28‰ and $\delta^{13}C_{carb}$ values reach nearly −1‰, reflecting intensified marine productivity under relatively stable paleoenvironmental conditions. Overall, both isotope curves exhibit similar long-term trends, although the $\delta^{13}C_{org}$ record shows sharper and more frequent fluctuations, whereas the $\delta^{13}C_{carb}$ curve remains comparatively smoother and reflects broader changes in the marine carbon reservoir.

4.5. $\delta^{18}O$ in AJ-02 core

The $\delta^{18}O$ values range from approximately −6‰ to −0.4‰ VPDB throughout the studied interval (**Fig. 4**). In the UC16a Zone (Upper Campanian; 70–64 m), values are relatively low, fluctuating between −3‰ and −6‰. Up-section, $\delta^{18}O$ values show a marked increase and remain generally between −0.4‰ and −3‰ from the UC16b Zone through the upper part of the UC19 Zone (64–~29 m). At approximately 28–29 m depth, near the transition between the upper UC19 Zone and the lower UC20a Zone, the curve shifts toward lower values. Above this level, $\delta^{18}O$ values decrease and remain relatively stable, ranging between −3‰ and −3.8‰ through the upper UC19 and lower UC20a intervals. Overall, the record indicates an increase in $\delta^{18}O$ values from the

https://doi.org/10.5194/egusphere-2026-3135
Preprint. Discussion started: 7 July 2026

Upper Campanian into the lower Maastrichtian, followed by a negative shift in the upper part of the succession.

4.6. Nitrogen isotope and Carbon / Nitrogen ratio in Aj-02

The nitrogen isotope ($\delta^{15}N$) and C/N ratio curves display distinct variations throughout the Maastrichtian succession and closely reflect changes in organic matter source and marine productivity (**Fig. 4**). The $\delta^{15}N$ values generally fluctuate between approximately 0‰ and 6‰, showing moderate variability through most of the section. In the lower interval, $\delta^{15}N$ values remain relatively stable with slight oscillations; however, a pronounced decline occurs near the 42 m level, where values decrease sharply to around 1–2‰. This interval coincides with the highest productivity phase recorded in the section and likely reflects intensified nutrient utilization and enhanced primary productivity under upwelling conditions. Above 42 m, the $\delta^{15}N$ curve gradually increases again with moderate fluctuations toward the upper Maastrichtian. Similarly, the C/N ratio curve shows noticeable stratigraphic variability, generally ranging between approximately 5 and 20. Higher C/N values dominate the lower part of the section, indicating a mixed organic matter source with increased terrestrial input. At approximately 42 m depth, the curve displays a marked decline, reaching its lowest values in the section. This decrease corresponds to the interval of maximum marine productivity and suggests increased contribution of marine algal organic matter associated with intensified upwelling conditions. Above this level, the C/N values gradually increase upward, indicating a return to more mixed organic matter input and relatively reduced marine productivity.

https://doi.org/10.5194/egusphere-2026-3135
Preprint. Discussion started: 7 July 2026

4.7. SA-01 to AJ-02 correlation

Figure 8 shows a high-resolution correlation between the SA-01 and AJ-02 wells based on calcareous nannofossil biostratigraphy, lithofacies, TOC content, and paleoecological proxies across the Campanian–Maastrichtian succession and the K/Pg boundary. The correlation is supported by the recognition of nannofossil biozones UC16–UC20 and the consistent occurrence of key biostratigraphic markers in both sections. Both wells display similar paleoecological trends, characterized by an overall increase in *Watznaueria* spp. abundance and a corresponding decline in cool-water taxa (*Arkhangelskiella* spp. and *Cribrosphaerella ehrenbergii*) through the Maastrichtian. A major assemblage turnover is recorded in the upper part of UC19, at approximately 90 m depth in SA-01 and 24.2 m depth in AJ-02. At this level, *Watznaueria* spp. increase abruptly from <30% to >50% of the assemblage, whereas cool-water taxa decrease from ~15% to <7%. Increased nannofossil abundance, higher species diversity, and greater proportions of the shallow-water taxon *Zeugrhabdotus* spp (**Fig. 5**) also characterize this interval. The turnover occurs near the transition from the organic-rich, high-TOC interval to overlying low-TOC chalky deposits. Calcareous nannofossil assemblages and $\delta^{18}O$ data consistently indicate relatively cool conditions throughout the UC16–UC19 interval, followed by the onset of warming at the top of UC19 that persists through UC20 (**Fig. 8**). This warming phase is reflected by the decline of cool-water taxa and decreasing $\delta^{18}O$ values. The synchronous response of biotic and geochemical proxies in both wells indicates a regional late Maastrichtian warming event starting from upper UC19 to UC20.

https://doi.org/10.5194/egusphere-2026-3135
Preprint. Discussion started: 7 July 2026

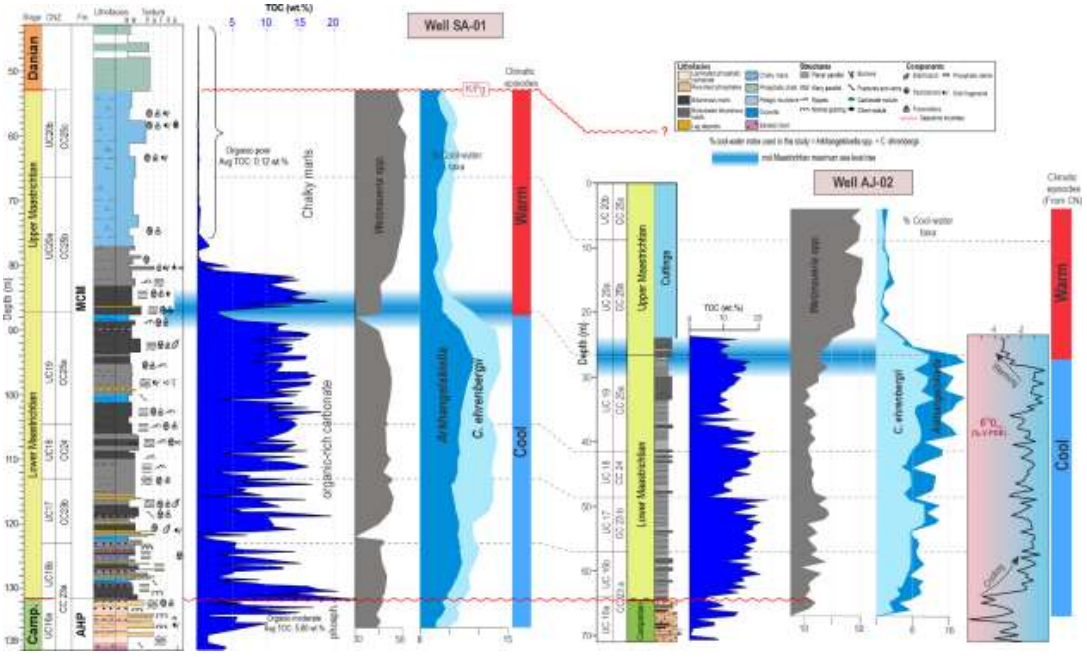

Figure 8. Integrated lithostratigraphic, geochemical, and calcareous nannofossil paleoecological interpretation of the SA-01 and AJ-02 cores across the upper Campanian–Maastrichtian to lower Danian succession. The figure illustrates variations in lithofacies, TOC content, organic-rich carbonate deposition, and the distribution of selected nannofossil taxa, particularly *Watznaueria* spp., *Arkhangelskiella* spp., and *Cribrosphaerella ehrenbergii*. Increased abundances of cool-water taxa during the lower Maastrichtian indicate cooler and nutrient-rich surface-water conditions associated with enhanced productivity and organic matter accumulation. Up-section, the gradual decline of cool-water taxa and the expansion of warm-water assemblages reflect progressive warming and more oligotrophic conditions during the late Maastrichtian and early Danian. The inferred K/Pg boundary and major climatic episodes are highlighted, together with the transition from phosphogenic intervals to carbonate-dominated sedimentation in both cores.

4.8. Cyclostratigraphy

A 4π-MTM spectral analysis was conducted on the gamma-ray (GR) records from the Maastrichtian succession of borehole SA-01 in Jordan in order to identify astronomically forced sedimentary cyclicities (**Fig. 7**). Background noise was estimated using a running median, and a red-noise model was calculated to determine confidence levels based on the χ^2 distribution. Although spectral peaks above the 95% confidence level are considered significant, a more conservative confidence threshold of 99% was adopted in this study. The spectral analysis of the

https://doi.org/10.5194/egusphere-2026-3135
Preprint. Discussion started: 7 July 2026

603 GR records reveals several significant cyclicities with confidence levels commonly exceeding
604 99%. The most prominent wavelengths occur at approximately 6.8 m, 1.6 m, and between 0.5 and
605 0.2 m. The ratios between these wavelengths closely correspond to the expected ratios of
606 Milankovitch orbital cycles, supporting their astronomical origin. Based on the estimated
607 sedimentation rates ranging between 1.5 and 2.3 cm/kyr, the 6.8 m cycle is interpreted as the long
608 eccentricity cycle (405 kyr), the 1.6 m cycle corresponds to short eccentricity (~100 kyr), and the
609 0.5–0.2 m wavelengths represent precession cycles (~20 kyr).

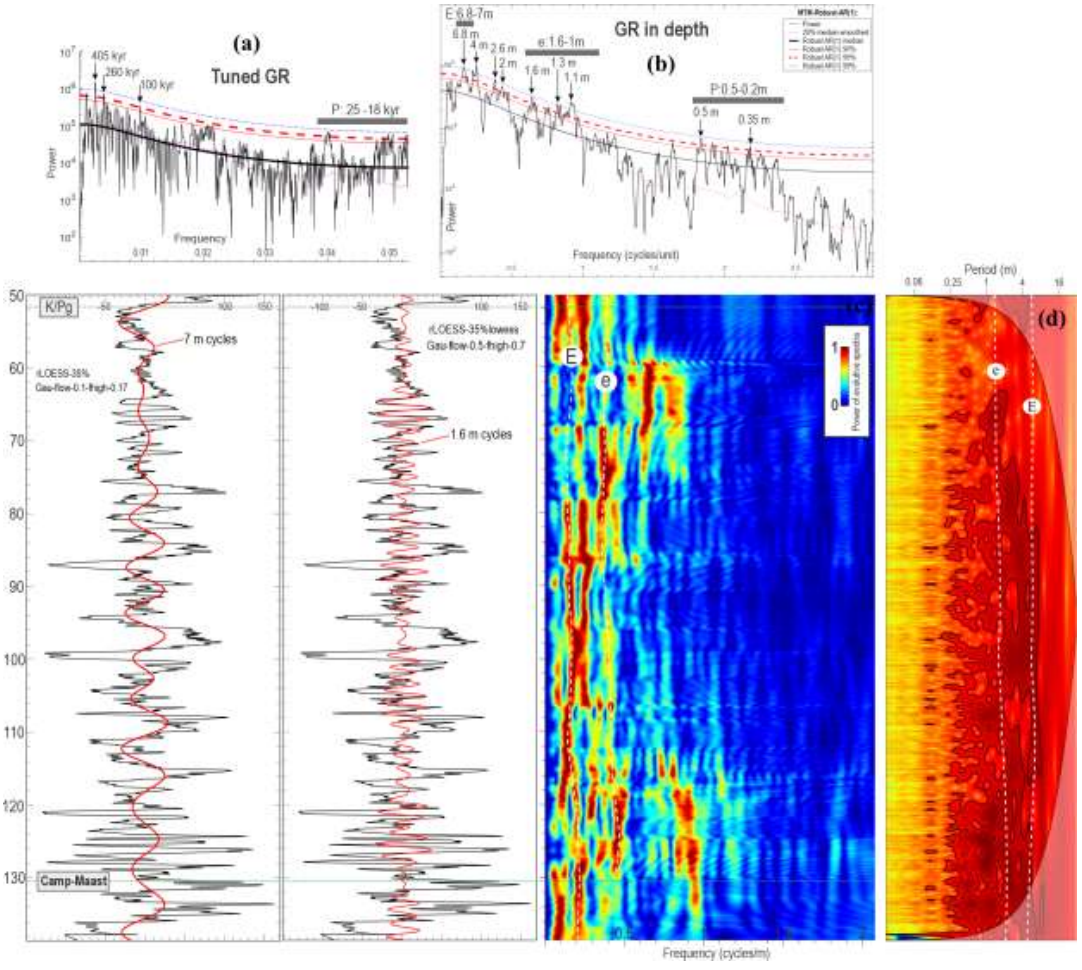

610

https://doi.org/10.5194/egusphere-2026-3135
Preprint. Discussion started: 7 July 2026

Figure 9. *Spectral and evolutive cyclostratigraphic analysis of the tuned gamma-ray (GR) record from the Maastrichtian oil shale succession in Jordan, illustrating orbital forcing of organic matter accumulation and upwelling dynamics along the southern Neo-Tethyan margin. (a) Multitaper method (MTM) power spectrum of the tuned GR series showing statistically significant cyclicities corresponding to the 405 kyr long eccentricity cycle, the ~100 kyr short eccentricity cycle, and the ~20 kyr precession band. The dominance of eccentricity-modulated precession suggests strong control of low-latitude insolation forcing on depositional processes. (b) High-frequency spectral analysis in depth domain identifying sedimentary expressions of eccentricity (E) and precession (P) cycles. The observed cyclic thicknesses are interpreted as variations in productivity, terrigenous influx, and preservation of organic matter driven by orbital forcing. (c) Evolutive wavelet spectrum of the GR series showing persistent eccentricity pacing through the studied interval, with intervals of enhanced precession power during phases of intensified climatic variability. The strengthening of precessional cyclicity upward is interpreted to reflect increasing sensitivity of the southern Neo-Tethyan climate system to ITCZ migration and monsoonal forcing during the Middle Maastrichtian Warming Event. (d) Wavelet power spectra show dominant eccentricity and precession cyclicities. High eccentricity periods amplified precessional forcing, strengthening seasonal insolation contrasts, northward ITCZ migration, and monsoon-driven upwelling along the southern Tethyan margin. Enhanced upwelling increased nutrient supply, productivity, and the expansion of oxygen-depleted, high-TOC depositional environments into the Jordanian Basin. In contrast, low eccentricity intervals weakened precessional forcing, reducing upwelling intensity and organic matter preservation. The shift toward stronger precession-driven variability at the onset of the Middle Maastrichtian Warming Event reflects enhanced coupling between tropical circulation, monsoonal dynamics, and marine productivity in the Neo-Tethys.*

The untuned GR series was further filtered within the bandwidth corresponding to the interpreted precession cycles. Amplitude modulation analysis of the filtered signal indicates that precession cycles are modulated by eccentricity cycles, producing groups of repetitive higher-frequency oscillations throughout the Maastrichtian succession. Subsequent 2π-MTM analysis performed on the amplitude envelope of the filtered series reveals strong spectral peaks within both the long and short eccentricity bands, well above the 99% confidence level. These results confirm the robustness of the interpreted orbital cyclicities identified in the MTM spectra. Continuous Wavelet Transform (CWT) and evolutionary Fast Fourier Transform (evoFFT) analyses further demonstrate that the long eccentricity cycle is the dominant astronomical signal within the Maastrichtian GR records (**Fig. 8**). The 6.8 m cycle exhibits the highest spectral power and remains persistent throughout most of the studied interval. Variations in cycle thickness

https://doi.org/10.5194/egusphere-2026-3135
Preprint. Discussion started: 7 July 2026

observed in the evoFFT spectrograms likely reflect minor fluctuations in sediment accumulation rates during deposition. The strong and continuous expression of the 405 kyr eccentricity cycle indicates that orbital forcing exerted a major control on sedimentation, marine productivity, and depositional conditions during the Maastrichtian in Jordan.

5. Discussion

5.1. Calcareous nannofossil paleoecology and Maastrichtian climate evolution

Calcareous nannofossil assemblages provide valuable insights into sea-surface temperature fluctuations and surface-water fertility during the Maastrichtian, as the distribution of many taxa is strongly controlled by climatic and oceanographic conditions (Eshet & Almogi-Labin, 1996; Püttmann et al., 2018; Püttmann & Tobias, 2021; Razmjooei et al., 2020; Thibault & Gardin, 2006b; Thibault & Husson, 2016). The assemblages recovered from the studied succession reveal a distinct paleoenvironmental evolution characterized by an early Maastrichtian cooling phase followed by a middle Maastrichtian warming event. The lower part of the succession, corresponding to the organic-rich oil shale interval (UC16 to UC19), contains relatively abundant *Arkhangelskiella* spp., *Cribrosphaerella ehrenbergii*, *Micula murus*, and *Micula staurophora*. Increased abundances of *Arkhangelskiella* and *C. ehrenbergii* are commonly regarded as indicators of cooler surface waters and have been widely used as proxies for high-latitude water influence during the Maastrichtian (Thibault and Gardin, 2007; Thibault et al., 2016). Their prominence within the early Maastrichtian interval therefore suggests that deposition occurred during a period of regional cooling superimposed on the overall Late Cretaceous greenhouse climate.

This interpretation is consistent with observations from the Zagros Basin, Iran, where Razmjooei et al. (2018) documented a pronounced increase in *Arkhangelskiella* spp. and *C.*

https://doi.org/10.5194/egusphere-2026-3135
Preprint. Discussion started: 7 July 2026

ehrenbergii across the lower Maastrichtian and interpreted these assemblage changes as evidence of cooler sea-surface conditions. Similar cooling trends have also been recognized in Boreal sections of northern Europe, where Thibault et al. (2016) identified a major early Maastrichtian cooling episode associated with increasing abundances of cool-water taxa and a decline in warm-water *Watznaueria* species. The occurrence of comparable assemblages in Jordan suggests that this cooling event was not restricted to the Boreal Realm but extended into the southern Neo-Tethyan margin, although local upwelling processes may have amplified its expression.

In contrast, the middle Maastrichtian chalk interval is characterized by a marked increase in *Watznaueria* spp. accompanied by a decline in *Arkhangelskiella* spp. and *C. ehrenbergii*. The dominance of *Watznaueria*, a taxon generally associated with warm, oligotrophic surface waters, indicates a return to more stable and warmer conditions. This assemblage turnover is interpreted as recording the Middle Maastrichtian warming event, a climatic phase recognized globally between the early and late Maastrichtian cooling episodes. Similar shifts toward warm-water assemblages have been reported from both the Zagros Basin (Razmjooei et al., 2018) and Boreal successions (Thibault et al., 2016), where temporary warming was associated with a reduction in cool-water indicators and a re-expansion of oligotrophic nannoplankton communities. In addition to temperature changes, variations in nutrient availability during the Middle Maastrichtian Event (UC19-UC20) are reflected by fluctuations in fertility-sensitive taxa such as *Zeugrhabdotus* spp. and *Biscutum* spp and increased continental run-off as shown by Ardila-Sanchez et al., (2026 accepted). The coexistence of productivity-indicating taxa with cool-water assemblages during the early Maastrichtian supports a scenario in which intensified upwelling and cooler surface waters promoted high biological productivity and contributed to the accumulation of organic-rich sediments (**Fig. 3**). This interpretation is consistent with geochemical evidence indicating

https://doi.org/10.5194/egusphere-2026-3135
Preprint. Discussion started: 7 July 2026

enhanced water-column stratification and elevated organic-matter preservation during deposition of the oil shale member (Usman et al., 2025). Calcareous nannofossil record documents a transition from relatively cool and productive surface-water conditions during the early Maastrichtian to warmer and more oligotrophic conditions during the Middle Maastrichtian (upper UC19-UC20).

5.2. Dinoflagellate cyst assemblages and the peridinioid/gonyaulacoid ratio

Biostratigraphically, the abundance of *Alterbidinium varium*, together with the occurrence of *Andalusiella mauthei* and *Senegalinium macroocystum*, indicates an Early Maastrichtian age (Slimani et al., 2000; Williams et al., 2004; Fensome et al., 2009). Additional taxa, including *Odontochitina operculata*, *Xenascus ceratioides*, and *Palaeohystrichophora infusorioides*, further constrain the succession to the Campanian–Maastrichtian transition. During the Late Campanian in Jordan and Nagev deposition was characterized by phosphatic-rich, siliceous sediments containing abundant chert nodules, silicified horizons, brecciated cherts, and porcellanites, indicating a significant contribution from siliceous plankton (Ashckenazi-Polivoda et al., 2011; Ashckenazi, 2012; Messaoud et al., 2025; Moshkovitz et al., 1983). Biomarker data from the Jurf Ed-Darawish oil shale deposits in Jordan, support this interpretation, showing high abundances of C25 isoprenoid thiophenes (diatom biomarkers) during the Campanian, followed by a marked decline across the Campanian–Maastrichtian boundary (Meilijson et al., 2014). C_{37} 2,5-dialkylthiophenes, indicative of Prymnesiophyte algae including coccolithophores, increase in abundance during the Early Maastrichtian, reflecting a shift toward calcareous nannoplankton-dominated productivity in Negev (Meilijson et al., 2014). The uppermost Campanian–Early Maastrichtian interval is dominated by peridinioid taxa such as *Alterbidinium*, *Andalusiella*, *Isabelidinium*, and *Senegalinium*, resulting in high peridinioid/gonyaulacoid (P/G) ratios. Because peridinioid dinocysts are mainly heterotrophic forms associated with nutrient-rich waters and

https://doi.org/10.5194/egusphere-2026-3135
Preprint. Discussion started: 7 July 2026

elevated primary productivity, their dominance indicates intense coastal upwelling and enhanced nutrient supply along the southern Neo-Tethyan margin. The scarcity of terrestrial palynomorphs suggests that nutrient enrichment was primarily marine in origin rather than related to increased continental runoff in the UC17 to lower UC19 interval. These conditions favored high organic carbon accumulation and the development of the organic-rich chalk and oil-shale facies characteristic of the Lower Maastrichtian. A major environmental change occurred near the Early–Middle Maastrichtian boundary, the dinoflagellate cyst record reflects this transition through a reduction in the dominance of heterotrophic peridinioid taxa and lower P/G ratios, suggesting diminished upwelling intensity, reduced nutrient availability, and decreased organic matter preservation. The change from highly productive (UC16 to UC19 zones), nutrient-enriched conditions to less productive (Upper UC19 and UC20 zones) is consistent with the reduction in TOC values and the disappearance of widespread organic-rich facies. The observed increase of terrestrial palynomorphs suggests that nutrient enrichment in the chalky marls unit (**Fig. 3**) was related to increased continental runoff during the Middle Maastrichtian warming event. The assemblages also exhibit mixed paleobiogeographic affinities, combining temperate peridinioid taxa with tropical Tethyan forms and rare Boreal elements such as *Laciniadinium* and *Palynodinium grallator*. Similar associations have been documented from Morocco and elsewhere within the Tethyan realm and are interpreted as evidence of intermittent incursions of cooler water masses linked to fluctuations in thermohaline circulation and regional current systems during the Campanian–Maastrichtian transition (Soncini, 1990; Slimani et al., 2016; Barron, 1987; Friedrich and Meier, 2006). Overall, the dinoflagellate cyst record documents the evolution from a highly productive upwelling-driven system during the Early Maastrichtian to less productive conditions

https://doi.org/10.5194/egusphere-2026-3135
Preprint. Discussion started: 7 July 2026

following the Early–Middle Maastrichtian transition, in agreement with changes recorded by TOC, lithofacies, biomarkers, and calcareous nannofossil assemblages.

5.3. $\delta^{13}C$ stratigraphy and recognition of the Middle Maastrichtian Event

A prominent feature of the Maastrichtian carbonate isotope record in Jordan is the predominance of negative δ^{13}Ccarb values relative to expected Maastrichtian seawater compositions. These depleted values are largely attributed to diagenetic alteration associated with the exceptionally organic-rich Maastrichtian oil shales, which commonly contain >20% TOC (Beik et al., 2018). Oxidation of organic matter during early diagenesis released isotopically light carbon 12 into pore waters, leading to carbonate recrystallization with lower $\delta^{13}C$ values, consistent with the pore-water alteration model of Lehmann et al. (2002). In some intervals, even more negative values suggest a second phase of alteration involving continued oxidation and secondary carbonate precipitation (Lehmann et al., 2002; Voigt et al., 2012). The weak correlation between $\delta^{13}C_{(carb)}$ and $\delta^{13}C_{(org)}$ indicates partial decoupling of inorganic and organic carbon reservoirs. While carbonate isotopes were affected by diagenesis, restricted circulation, stratification, and productivity changes, $\delta^{13}C_{(org)}$ values remained relatively stable around −29‰. These depleted organic carbon values likely reflect preferential degradation of C13-enriched compounds during early diagenesis, leaving behind isotopically lighter organic matter (Voigt et al., 2012). The Campanian–Maastrichtian Boundary Event (CMBE) is a globally recognized ~2.5 Myr negative carbon isotope excursion associated with Campanian–Maastrichtian cooling and recorded in Italy, the Pacific Ocean, and numerous Tethyan sections (e.g., Linnert et al., 2017). Three shorter positive excursions (Figs. 3 and 10, CMBE-a, b, and c) are superimposed on this trend and are interpreted as responses to long-eccentricity forcing (Voigt et al., 2012). In the AJ-02 core, CMBE occurs within nannofossil biozones UC16 and UC17. Correlation is constrained by the LO of

https://doi.org/10.5194/egusphere-2026-3135
Preprint. Discussion started: 7 July 2026

Tranolithus orionatus, the LO of *Broinsonia parca parca* below the excursion, and the FO of *Reinhardtites levis* above it (Alqudah et al., 2015). These bioevents correspond closely to the global CMBE framework spanning UC16–UC18 (Voigt et al., 2012). The negative isotope excursion of the CMBE has been linked either to oxidation of exposed organic-rich sediments during Maastrichtian regression (Jarvis et al., 2006) or to enhanced ventilation by oxygen-rich deep waters that reduced organic carbon burial (e.g., Jung et al., 2013; Thibault et al., 2016).

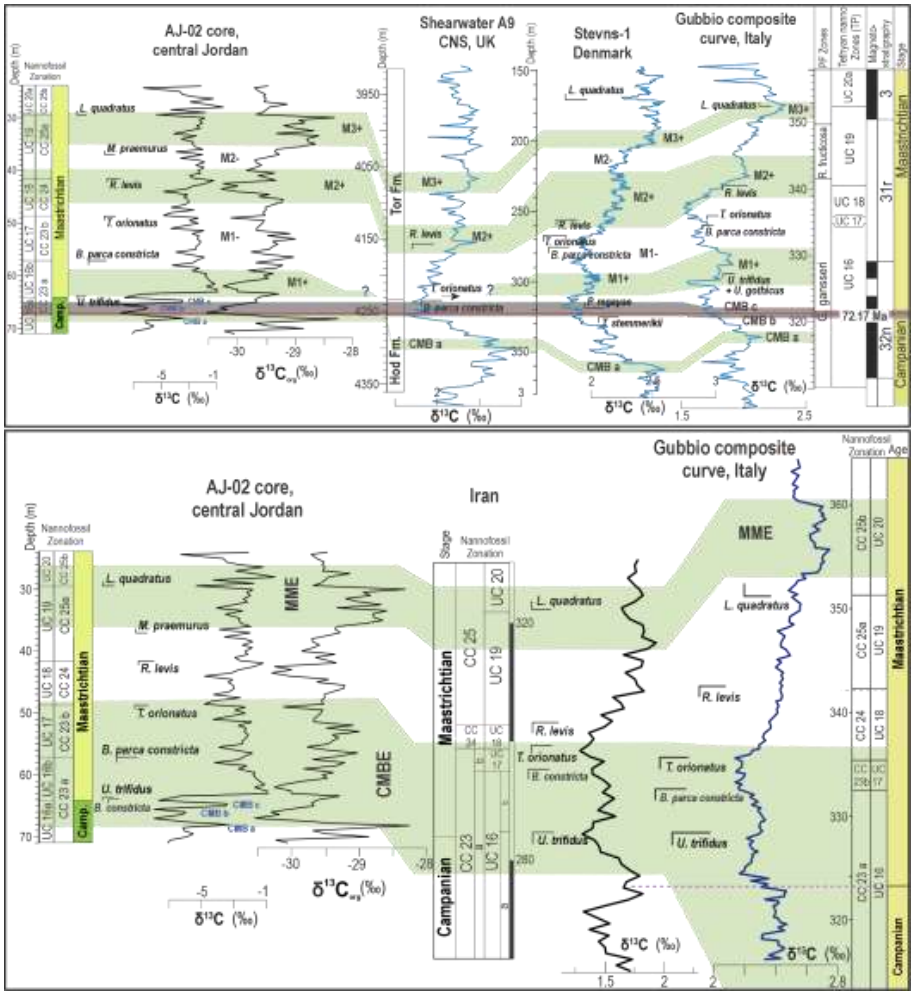

Figure 10. *Correlation of the AJ-02 core (central Jordan) with regional and global carbon isotope stratigraphic records across the late Campanian–Maastrichtian interval. The upper panel*

https://doi.org/10.5194/egusphere-2026-3135
Preprint. Discussion started: 7 July 2026

compares the AJ-02 δ¹³C curve and calcareous nannofossil zonation with reference sections from Shearwater A9 (CNS, UK), Stevns-1 (Denmark), and the Gubbio composite curve (Italy). Major positive and negative carbon isotope excursions (M1+, M1−, M2+, M2−, and M3+) are correlated between sections together with key biostratigraphic marker taxa, including Uniplanarius trifidus, Broinsonia parca constricta, Tranolithus orionatus, Reinhardtites levis, Micula praemurus, *and* Lithraphidites quadratus. *The Campanian–Maastrichtian boundary (CMB a–c) and the interpreted age of 72.17 Ma are indicated. The lower panel illustrates the correlation of the AJ-02 isotope record with Maastrichtian successions from Iran and the Gubbio composite section, emphasizing the Maastrichtian Mid-Event (MME) and the Campanian–Maastrichtian Boundary Event (CMBE). Integrated carbon isotope stratigraphy and calcareous nannofossil biozonation demonstrate the regional and global consistency of the AJ-02 succession and provide a refined chronostratigraphic framework for the Maastrichtian deposits of central Jordan.*

Between ~69 and 68 Ma, the Middle Maastrichtian warming event is recorded in Jordan and is not identified solely from carbon-isotope stratigraphy. Although it is associated with coupling between the $\delta^{13}C_{carb}$ and $\delta^{13}C_{org}$ records (**Fig. 10**), its recognition is further supported by calcareous nannofossil biostratigraphy, the astronomically calibrated age model, and quantitative nannofossil paleoecology, which documents a pronounced warming signal (**Figs. 8 and 10**). This dual expression provides strong evidence that the event reflects a primary paleoenvironmental signal rather than solely diagenetic modification. In the AJ-02 core, MME-1 is represented by a positive excursion at approximately 69 Ma, followed by the negative MME-2 excursion at 68.6 Ma. Importantly, the FO of *Lithraphidites quadratus* within the MME (68.6 Ma in Jordan), precisely matching its position relative to the MME in the Gubbio reference section (**Fig. 10**, Voigt et al., 2012). Biostratigraphically, the MME is constrained by the FO of *Lithraphidites quadratus* and occurs below the FO of *Micula murus*. The event occupies the upper UC19–UC20 interval and therefore provides an important chronostratigraphic marker throughout the Neo-Tethys. The MME is also clearly expressed in the organic carbon isotope record. Throughout most of the oil shale member, δ^{13}Corg values remain stable at approximately −29‰, indicating persistent stratification and stable greenhouse conditions. However, at the top of the oil shale member, $\delta^{13}C_{org}$ shifts positively by nearly 2‰ (**Fig. 10**). This isotopic shift coincides with changes in $\delta^{13}C_{carb}$ and is

https://doi.org/10.5194/egusphere-2026-3135
Preprint. Discussion started: 7 July 2026

interpreted as evidence for improved bottom-water ventilation and increased degradation of previously preserved organic matter. Consequently, MME-1 correspond to intervals of elevated TOC values and enhanced organic matter preservation, whereas MME-2 reflects a brief episode of increased ventilation and oxidation before the complete shift to chalk during the Late Maastrichtian (UC20 zone).

5.4. Nitrogen isotopes and organic matter accumulation

Nitrogen isotopes and elemental geochemistry provide important insights into the mechanisms controlling organic matter accumulation and preservation within the Maastrichtian oil shales of Jordan. The succession is characterized by high TOC values, low total organic nitrogen (TON) concentrations, and exceptionally elevated C/N ratios that commonly exceed 25 (**Fig. 3**). While such values are often interpreted as evidence of increased terrestrial organic matter input, petrographic, geochemical, and biomarker (Usman et al., 2025) with our palynologiacal data in this study indicate that the organic matter is predominantly marine and algal in origin. Consequently, the elevated C/N ratios are more likely the result of preferential degradation and loss of nitrogen-rich organic compounds during early diagenesis rather than enhanced terrestrial contribution. Similar geochemical characteristics have been reported from organic-rich marine sediments and modern coastal upwelling systems, such as the Benguela and Peru margins, where intense recycling and removal of nitrogen-bearing compounds significantly modify the original elemental composition of organic matter (e.g., Meyers et al., 2006; Twichell et al., 2002).

The most pronounced geochemical change occurs near the 40 m level, where a rapid decrease in C/N ratios coincides with a marked negative excursion in $\delta^{15}N$ values (**Fig. 4**). This interval corresponds broadly to the highly organic-rich Cycle 2 recognized in the Maastrichtian succession

https://doi.org/10.5194/egusphere-2026-3135
Preprint. Discussion started: 7 July 2026

and interpreted by Usman et al. (2025) as representing a period of intensified productivity coupled with strongly reducing, anoxic to euxinic bottom-water conditions. The concurrent decrease in $\delta^{15}N$ and C/N ratios suggests substantial alteration of the primary nitrogen signal during deposition and early burial. Under persistent euxinic conditions, enhanced degradation of nitrogen-rich organic compounds and intensified microbial nitrogen cycling likely promoted the preferential removal of sedimentary nitrogen relative to carbon, resulting in low TON values and elevated C/N ratios. Such processes would effectively overprint the original marine nitrogen isotopic composition and contribute to the exceptional preservation of organic carbon.

The $\delta^{15}N_{org}$ record further supports a strong influence of oxygen-deficient conditions on nitrogen cycling throughout the succession. Relatively depleted $\delta^{15}N$ values within the upper Phosphate Member and lower oil shale interval indicate extensive nitrogen transformation under low-oxygen conditions, potentially involving denitrification and anammox processes within the water column and sediment pore waters. These pathways are commonly associated with expanded oxygen minimum zones and enhanced nutrient recycling in productive marine settings. The observed relationship between $\delta^{15}N$ values and C/N ratios therefore points to a close coupling between nitrogen cycling, redox conditions, and organic matter preservation during deposition of the Maastrichtian oil shales. Collectively, the geochemical and micropaleontological data indicate that organic matter enrichment in the Maastrichtian oil shales of Jordan was controlled by the interplay of enhanced upwelling-driven productivity, persistent water-column stratification, and dysoxic to euxinic conditions. The pronounced shift in nitrogen isotopes and elemental ratios near the 40 m level records a critical interval of intensified oxygen depletion and nitrogen loss, coinciding with maximum organic carbon accumulation an minimum sedimentation rate. These conditions promoted exceptional preservation of marine organic matter and contributed to the

https://doi.org/10.5194/egusphere-2026-3135
Preprint. Discussion started: 7 July 2026

development of one of the most organic-rich Maastrichtian depositional systems along the southern Neo-Tethyan margin (Usman et al., 2025; Twichell et al., 2002; Meyers et al., 2006).

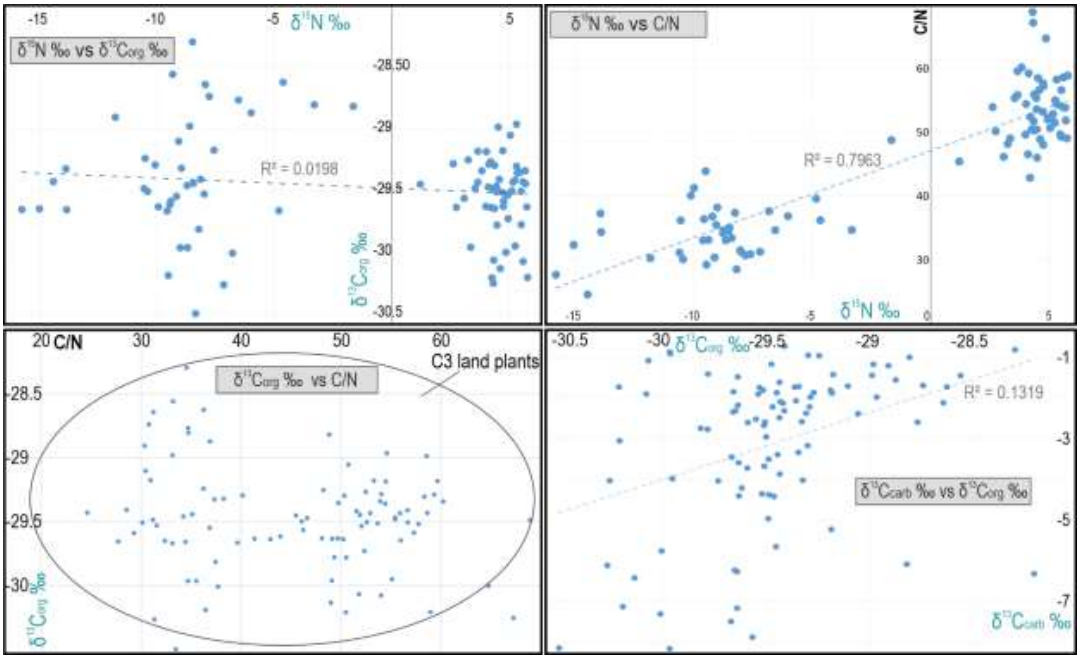

Figure 11. *Cross-plots illustrating relationships between stable isotopes and organic geochemical proxies from the studied Maastrichtian oil shale succession. The diagrams compare $\delta^{15}N$ values with $\delta^{13}C_{org}$, C/N ratios, and $\delta^{13}C_{ar}b$, together with the relationship between $\delta^{13}C_{org}$ and C/N ratios. The weak correlation between $\delta^{15}N$ and $\delta^{13}C_{org}$ (R^2 = 0.0198) suggests that nitrogen isotopic variations were largely independent of changes in organic carbon isotopic composition. In contrast, $\delta^{15}N$ shows a strong positive correlation with C/N ratios (R^2 = 0.7963), indicating a close relationship between nitrogen cycling and the source or preservation of organic matter. The $\delta^{13}C_{org}$ versus C/N plot indicates predominantly marine organic matter input with minor terrestrial influence, although some samples trend toward higher C/N values consistent with limited contribution from C3 land plants. The weak correlation between $\delta^{13}C_{ar}b$ and $\delta^{13}C_{org}$ (R^2 = 0.1319) suggests partial decoupling between carbonate and organic carbon reservoirs, likely reflecting variations in productivity, diagenesis, and organic matter preservation under fluctuating paleoenvironmental conditions.*

5.5. Orbital forcing, upwelling cyclicity, and relative sea-level rise

The Mid-Maastrichtian Event (MME) represented a major greenhouse perturbation that reorganized sea level, ocean circulation, productivity, and carbon burial across the southern Neo-Tethys (e.g., Chauris et al., 1998; Dubicka et al., 2024). The event was associated with a long-

https://doi.org/10.5194/egusphere-2026-3135
Preprint. Discussion started: 7 July 2026

lived eustatic transgression lasting approximately 2 Myr and reaching several tens of meters, likely on the order of 50–70 m and potentially approaching 100 m in some regions, as inferred from planktonic foraminiferal depth distributions and sequence-stratigraphic reconstructions from the European shelf seas (Dubicka et al., 2024; Kominz et al., 2008; Pearson et al., 2001). This transgression corresponds to the globally recognized Maastrichtian transgressive peak near the lower–upper Maastrichtian boundary and was accompanied by significant changes in ocean circulation and marine connectivity (Thibault et al., 2012; Dubicka et al., 2024). In Jordan, the MME-related sea-level rise would have increased accommodation space across the southern Neo-Tethyan shelf, expanded deeper-water environments, and altered the spatial distribution of productivity centers and organic-matter preservation. The initial phase of transgression may have enhanced continental runoff and nutrient delivery through intensified weathering and flooding of low-relief continental areas, a process documented elsewhere by increased terrestrial organic-matter input, radiogenic osmium excursions, elevated C/N ratios, and geochemical indicators of enhanced hydrological activity (Dubicka et al., 2024; Usman et al., 2025). Such a scenario is consistent with intensified greenhouse conditions during the MME and supports the interpretation that nutrient supply to the Jordanian shelf became increasingly influenced by runoff-derived inputs in addition to classical wind-driven upwelling. The climatic forcing behind this reorganization was likely related to elevated atmospheric CO_2 concentrations and global warming associated with enhanced volcanic activity (Dubicka et al., 2024). Multiple studies have linked the MME to emplacement of large igneous provinces, particularly volcanic activity associated with the Kerguelen hotspot and Ninetyeast Ridge, and possibly the earliest phase of Deccan volcanism(Dubicka et al., 2024). These volcanic episodes may have released substantial quantities of greenhouse gases, driving warming, intensifying the hydrological cycle, and contributing to

https://doi.org/10.5194/egusphere-2026-3135
Preprint. Discussion started: 7 July 2026

eustatic sea-level rise through oceanic plateau emplacement and thermal uplift of the seafloor (Dubicka et al., 2024). The effects of the MME in Jordan therefore likely extended beyond simple changes in upwelling intensity. Enhanced greenhouse conditions, rising sea level, and a strengthened hydrological cycle would have modified nutrient pathways and basin circulation patterns, producing a gradual reorganization of productivity regimes across the southern Neo-Tethyan shelf. This interpretation is consistent with the findings of Ardila-Sanchez et al., 2026 accepted), who proposed a fundamental shift in the dominant nutrient source at the Early–Late Maastrichtian transition, from a productivity system primarily sustained by wind-driven upwelling to one increasingly supported by continental runoff and terrigenous nutrient delivery.

The pronounced cyclicity observed within the Maastrichtian oil shale succession shows the preservation of orbital-scale forcing (short eccentricity) of the southern Neo-Tethyan upwelling system. Alternations between organic-rich and organic-poor intervals are interpreted as the sedimentary expression of eccentricity-modulated precessional climate variability (**Fig. 12**). During intervals of high orbital eccentricity, precessional forcing amplified seasonal contrasts in insolation. When perihelion occurred during Northern Hemisphere summer, intensified summer heating strengthened monsoonal circulation and promoted northward migration of the Intertropical Convergence Zone (ITCZ). These climatic conditions enhanced wind-driven coastal upwelling along the southern Neo-Tethyan margin, transporting nutrient-rich deep waters into the photic zone and stimulating exceptional marine productivity. Enhanced productivity increased the export flux of organic matter to the seafloor, while intensified water-column stratification promoted development of dysoxic to anoxic bottom-water conditions. These intervals correspond to deposition of high-TOC laminated oil shales. In contrast, weaker monsoonal circulation during opposite precessional configurations reduced upwelling intensity, enhanced bottom-water

https://doi.org/10.5194/egusphere-2026-3135
Preprint. Discussion started: 7 July 2026

908 ventilation, and favored deposition of more carbonate-rich marl and chalk facies. Relative sea-
909 level rise further modified the expression of these orbitally driven cycles.

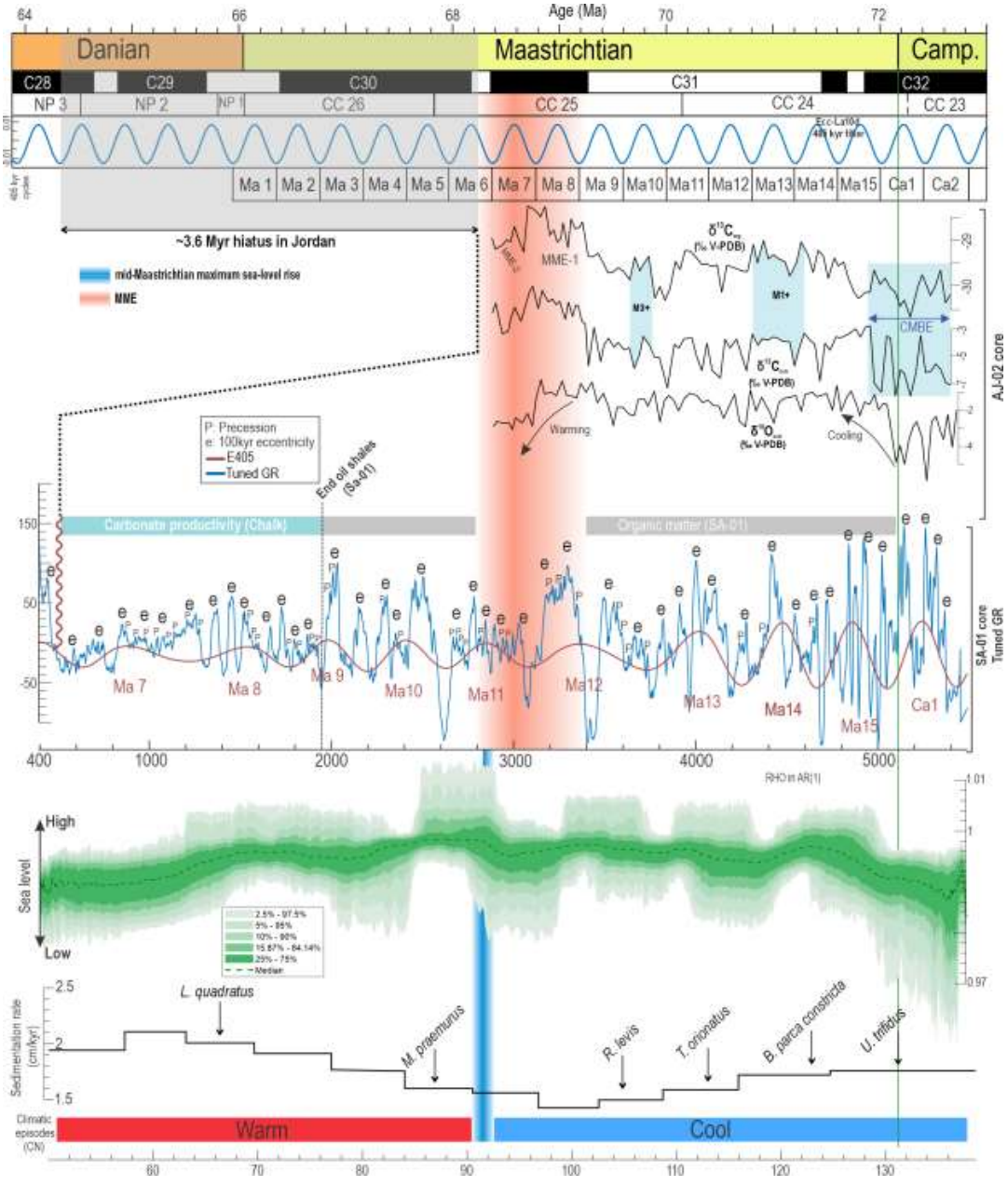

910

https://doi.org/10.5194/egusphere-2026-3135
Preprint. Discussion started: 7 July 2026

Figure 12. *Integrated astrochronological, paleoceanographic, and geochemical framework for the Maastrichtian upwelling system along the southern Neo-Tethyan margin. The figure combines orbital-scale cyclicity derived from gamma-ray (GR) records with carbon isotope stratigraphy, calcareous nannofossil bioevents, sea-level evolution, and reconstructed climatic conditions across the Campanian–Danian interval. The tuned GR signal reveals eccentricity–precession paced cyclicity corresponding to Maastrichtian depositional sequences (Ma1–Ma15), interpreted as fluctuations in productivity and redox conditions linked to orbitally forced changes in monsoonal circulation and coastal upwelling intensity. The interval of intensified upwelling during the early Maastrichtian coincides with cooler climatic conditions, enhanced nutrient delivery, elevated organic carbon burial, and development of oxygen-deficient bottom waters. A middle Maastrichtian warming event (MME) is associated with progressive weakening and eastward migration of the upwelling system, accompanied by rising sea level and reduced productivity in western Jordan. Biostratigraphic calibration is based on calcareous nannofossil zones (CC22–NP3), including the Campanian–Maastrichtian boundary and the Early–Late Maastrichtian transition marked by key nannofossil events.*

The MME may record a redistribution of nutrient sources and productivity pathways, whereby orbital-scale upwelling cycles remained important but were progressively supplemented—and in some sub-basins replaced—by runoff-driven nutrient supply. Consequently, the diachronous termination of oil shale deposition across Jordan reflects the combined influence of orbital forcing, greenhouse warming and eustatic sea-level rise, volcanically driven perturbations to the carbon cycle, and hydrological intensification. While eccentricity-paced climate cycles continued to regulate short-term variations in productivity and redox conditions, the MME fundamentally altered basin-scale oceanography and nutrient delivery mechanisms, shifting the long-term balance from predominantly upwelling-controlled organic-carbon accumulation toward increasingly runoff-influenced and carbonate-dominated depositional systems.

Conclusion

Integrated micropaleontological, geochemical, and isotopic records from the Maastrichtian succession of Jordan reveal a highly dynamic southern Neo-Tethyan upwelling system controlled by the interplay of orbital forcing, climate change, sea-level fluctuations, and nutrient cycling. High productivity, recurrent oxygen depletion, and efficient organic matter preservation produced

https://doi.org/10.5194/egusphere-2026-3135
Preprint. Discussion started: 7 July 2026

exceptionally organic-rich oil shales, reflecting strong coupling between ocean circulation, carbon burial, and climate. Orbital-scale variability was primarily governed by eccentricity-modulated precession, which influenced ITCZ migration, regional wind patterns, and upwelling intensity. These processes controlled nutrient supply, productivity, and redox conditions, generating the characteristic alternation between organic-rich and carbonate-rich intervals. Superimposed on these cycles, the Mid-Maastrichtian Event (MME) triggered a major reorganization of the southern Neo-Tethyan system. Greenhouse warming intensified the hydrological cycle, altered atmospheric circulation, weakened and shifted the upwelling system eastward, and increased the importance of runoff-derived nutrients. As a result, depositional systems evolved from predominantly upwelling-driven oil shale accumulation during the Early Maastrichtian to increasingly carbonate-dominated sedimentation during the Late Maastrichtian. Rather than recording a collapse of productivity, the diachronous termination of oil shale deposition across Jordan reflects the migration of productive, oxygen-deficient depocenters in response to sea-level rise and changing nutrient pathways. The Maastrichtian oil shales of Jordan thus provide an important deep-time analogue for understanding how warming climates, intensified hydrological cycles, and expanding oxygen-deficient waters can reshape marine productivity and carbon burial.

Data availability

The authors confirm that the data supporting the findings of this study are available within the article's supplementary materials.

Declaration of Competing Interest

The authors declare that they have no known competing financial interests or personal relationships that could have appeared to influence the work reported in this paper.

https://doi.org/10.5194/egusphere-2026-3135
Preprint. Discussion started: 7 July 2026

Credit authorship contribution statement

All authors provided a direct scientific contribution to this article. **Jihede Haj Messaoud:** Conceptualization, Methodology, Software, Data analysis, Data Curation, Visualization, Investigation, writing – original draft, writing – review and editing. **Maria Ardila-Sanchez:** Conceptualization, Methodology, Data Curation, Investigation, writing – original draft. **Khalil, Ibrahim ;** Data Curation, Supervision, Project administration. **Israa Abu-Mafouz:** Data Curation, Funding acquisition, writing – original draft. **Volker Vahrenkamp:** Data Curation, and Investigation. **Frans van Buchem:** Conceptualization, Methodology, Software, Data analysis, Data Curation, Visualization, Investigation, writing – original draft, writing – review and editing, Supervision, Project administration.

Acknowledgments

This study was funded by King Abdullah University of Science and Technology (KAUST) through the baseline funding of FVB. We acknowledge the Ministry of Energy and Mineral Resources (MEMR), Karak International Oil (KIO), and Al-Qamer for Energy and Infrastructure Ltd., Jordan, for providing the core samples used in this study. The Hashemite University (Amman, Jordan) for its logistical support during the fieldtrips campaign. We also extend sincere thanks to Elhadj Marwane Diallo and Mahmoud Mowafi (Earth Science and Engineering program at KAUST) for their technical assistance with Rock-Eval analyses, as well as Samer Al Jurf for the kind assistance during the field work

Funding

This study was funded by King Abdullah University of Science and Technology (KAUST) through the baseline funding of FVB.

https://doi.org/10.5194/egusphere-2026-3135
Preprint. Discussion started: 7 July 2026

References

Abu-Mahfouz, I. S., Wicaksono, A. N., Idiz, E., Cartwright, J., Santamarina, J. C., and Vahrenkamp, V. C: Modelling the initiation of bitumen-filled microfractures in immature, organic-rich carbonate mudrocks: The Maastrichtian source rocks of Jordan. Marine and Petroleum Geology, 141. https://doi.org/10.1016/j.marpetgeo.2022.105700, 2022.

Alberti, G. Zur Kenntnis der Gattung Feldraede Eisenack (Dinoflag.) in der Kreide und im Alttertiär Nord- und Mitteldeutschlands. Mitteilungen aus dem Geologischen Staatsinstitut in Hamburg, v. 28, p. 93–105, pls. 8, 9. (In German.), 1959

Almogi-Labin, A., Bein, A., and Sass, E: Late Cretaceous upwelling system along the Southern Tethys Margin (Israel): Interrelationship between productivity, bottom water environments, and organic matter preservation. Paleoceanography, 8(5), 671–690. https://doi.org/10.1029/93PA02197, 1993.

Alqudah, M., Al Alaween, M., Fermor, A., Ali, E., Wagner, T., Alhakimi, M. H., and Rahim, A: Impact of Thermal Maturation of the Upper Cretaceous Bituminous Limestone of Attarat Um Ghudran Central Jordan on Calcareous Nannofossil Preservation. ACS Omega, 8(42), 39830–39846. https://doi.org/10.1021/acsomega.3c06033, 2023.

Alqudah, M., Ali Hussein, M., van den Boorn, S., Podlaha, O. G., and Mutterlose, J. Biostratigraphy and depositional setting of Maastrichtian–Eocene oil shales from Jordan, *Mar. Petrol. Geol.*, **60**, 87–104, 2015.

Ashckenazi, S: The Late Cretaceous Southern Tethyan Upwelling System: A Case Study from the High Productivity Sequence, Negev, Israel Sarit Ashckenazi-Polivoda., 2012.

Ashckenazi-Polivoda, S., Abramovich, S., Almogi-Labin, A., Schneider-Mor, A., Feinstein, S., Püttmann, W., and Berner, Z: Paleoenvironments of the latest Cretaceous oil shale sequence, Southern Tethys, Israel, as an integral part of the prevailing upwelling system. Palaeogeography, Palaeoclimatology, Palaeoecology, 305(1–4), 93–108. https://doi.org/10.1016/j.palaeo.2011.02.018, 2011.

Beik, I., Adatte, T., Podlaha, O. G., and Mutterlose, J: Maastrichtian to early Paleocene sea level changes and climatic evolution on the southeastern Tethys margin. Marine and Petroleum Geology, 100, 285–296. https://doi.org/10.1016/j.marpetgeo.2018.11.018, 2019.

Beik, I., Gómez, V. G., Podlaha, O. G., and Mutterlose, J: The δ13C record of Maastrichtian-Paleocene oil shales from Jordan – Stratigraphic and environmental implications for an epicontinental setting. Journal of African Earth Sciences, 143, 134–144. https://doi.org/10.1016/j.jafrearsci.2018.03.022, 2018.

Bijl, P.K. DINOTRAT: a global database of the stratigraphic and paleotidal distribution of Mesozoic–Cenozoic organic-walled dinoflagellate cysts. Earth System Science Data, v. 14, p. 579–617, 2022

Bou Daher, S., Nader, F. H., Müller, C., and Littke, R: Geochemical and petrographic characterization of Campanian-Lower Maastrichtian calcareous petroleum source rocks of Hasbayya, South Lebanon. Marine and Petroleum Geology, 64, 304–323. https://doi.org/10.1016/j.marpetgeo.2015.03.009, 2015.

Bou Daher, S., Nader, F. H., Strauss, H., and Littke, R: depositional environment and source-rock characterisation of organic-matter rich upper santonian-upper campanian carbonates, northern lebanon. In Journal of Petroleum Geology (Vol. 37, Number 1). www.jpg.co.uk, 2014.

Bown, P. R., and Young, J. R: Techniques. In: Bown, P.R. (Ed.), Calcareous Nannofossil Biostratigraphy. Chapman & Hall, London, 16–28., 1998.

https://doi.org/10.5194/egusphere-2026-3135
Preprint. Discussion started: 7 July 2026

Brinkhuis, H., Segers, S., Sluijs, A., Warnaar, J., Williams, G.L. 2003: Latest Cretaceous to earliest Oligocene, and Quaternary dinoflagellates from ODP Site 1172, East Tasman Plateau. In: Exon, N. & Kennett, J.P. (editors), Proceedings of the ODP, Scientific Results, Leg 189, U.S. Government Printing Office, College Station, Texas, p. 1–48.

Burnett, J. A: Upper Cretaceous. In Bown (Ed.) (Ed.), Calcareous Nannofossil Biostratigraphy (pp. 132–199)., 1998.

Catzanarti, R., Ellero, A., Levi, N., Otrio, G., Pandolfi, L. Calcareous nannofossil biostratigraphy of the Antola Unit succession (Northern Apennines, Italy): new age constraints for the Late Cretaceous Helminthoid Flysch. Cretaceous Research, v. 28, 841–860, 2007

Chauris, H., Lerousseau, J., Beaudoin, B., Propson, S., and Montanari, A: Inoceramid extinction in the Gubbio basin (northeastern Apennines of Italy) and relations with mid-Maastrichtian environmental changes. In Palaeogeography, Palaeoclimatology, Palaeoecology (Vol. 139)., 1998.

Cookson, I.C., Eisenack, A. Micropalynology from Australian Cretaceous sediments. Micropaleontology, v. 6, no. 1, p. 1–18, pls. 1–3, 1960

Coradini, D., Non-calcareous microplankton from the Upper Cretaceous of the northern Apennines. Bollettino del Museo Paleontologia Italiana, v. 11, p. 119–197, pls. 19–39, 1973

Costa, L.J., Davey, F.J. 1992: Dinoflagellate cysts of the Cretaceous System. In: Powell, A.J. (editor), A Stratigraphic Index of the Cretaceous cysts of the Upper Cretaceous, p. 99–131.

Crouch, E.M., Williams, P., Kulhanek, D.K., Gibbs, S. A revised Paleocene (Teurian) dinoflagellate cyst zonation from eastern New Zealand. Review of Palaeobotany and Palynology, v. 202, p. 477–492, 2014

Dubicka, Z., Wierny, W., Bojanowski, M. J., Rakociński, M., Walaszczyk, I., and Thibault, N: Multi-proxy record of the mid-Maastrichtian event in the European Chalk Sea: Paleoceanographic implications. Gondwana Research, 129, 1–22. https://doi.org/10.1016/j.gr.2023.11.010, 2024.

Edelman-Furstenberg, Y: Cyclic upwelling facies along the Late Cretaceous southern Tethys (Israel): taphonomic and ichnofacies evidence of a high-productivity mosaic. Cretaceous Research, 30(4), 847–863. https://doi.org/10.1016/j.cretres.2009.01.005, 2009.

Eshet, Y., and Almogi-Labin, A: Calcareous nannofossils as paleoproductivity indicators in Upper Cretaceous organic-rich sequences in Israel. In Marine Micropaleontology (Vol. 29)., 1996.

Ester, Y., Mokhbatiz, S., Habib, D., Benjamini, C., Margritz, M. 1996: Calcareous nannofossil and dinoflagellate stratigraphy across the Cretaceous/Tertiary boundary at Hof Hahai, Israel. Marine Micropaleontology, v. 11, p. 199–228.

Fensome, R.A., Crouch, E.M., Nonmarine dinoflagellate cysts of the Cretaceous System. In: Powell, A.J. (editor), A Stratigraphic Index of Dinoflagellates of the Upper Cretaceous, p. 99–131, 1991

Frank, T. D., Thomas, D. J., Leckie, R. M., Arthur, M. A., Brown, P. R., Jones, K., and Lees, J. A: The Maastrichtian record from Shatsky Rise (northwest Pacific): A tropical perspective on global ecological and oceanographic changes. Paleoceanography, 20(1), 1–14. https://doi.org/10.1029/2004PA001052, 2005.

Giraldo-Gómez, V. M., Beik, I., Podlaha, O. G., and Mutterlose, J: A paleoenvironmental analyses of benthic foraminifera from Upper Cretaceous – lower Paleocene oil shales of Jordan. Cretaceous Research, 91, 1–13. https://doi.org/10.1016/j.cretres.2018.04.021, 2018.

Heilmann-Clausen, C. Dinoflagellate stratigraphy of the uppermost Danian to Ypresian in the Viborg borehole, central Jutland, Denmark. Danmarks Geologiske Undersogelse, v. 7, p. 1–69, 1985

https://doi.org/10.5194/egusphere-2026-3135
Preprint. Discussion started: 7 July 2026

Hilly, R., Morgan, R. Australian marine Mesozoic and Cenozoic dinoflagellates. In: Jell, P.A. (editor), Studies in Australian Mesozoic Palynology, volume 4, Memories of the Association of Australasian Palaeontologists, p. 1–94, 1987

Jarvis, I., Gale, A. S., Jenkyns, H. C., and Pearce, M. A.: Secular variation in Late Cretaceous carbon isotopes: a new $\delta^{13}C$ reference curve for the Cenomanian–Campanian (99.6–70.6 Ma), *Geol. Mag.*, **143**, 561–608, 2006

Jung, C., Voigt, S., and Friedrich, O. High-resolution carbon-isotope stratigraphy across the Campanian–Maastrichtian boundary at Shatsky Rise (tropical Pacific), *Cretaceous Res.*, **37**, 177–185, 2012.

Kalifi, A., Haj Messaoud, J., Baby, G., Ibrahim, K., Powell, J. H., and van Buchem, F: Tectono-stratigraphic evolution of the Late Cretaceous-Eocene of Jordan and implications for the Arabian Plate convergent margin phase. Marine and Petroleum Geology, 181. https://doi.org/10.1016/j.marpetgeo.2025.107525, 2025.

Köthe, A. Dinoflagellatenzysten aus der Oberkreide des Helvetikum und Nordturalhelvetikum von Oberbayern. Münchner Geowissenschaftliche Abhandlungen, Reihe A, Geologie und Paläontologie, v. 22, p. 1–306, pls. 1–43. (In German.), 1992.

Köthe, A. 2012: A revised Cenozoic dinoflagellate cyst and calcareous nannoplankton zonation for the German sector of the southern North Sea Basin. Newsletters on Stratigraphy, v. 45, no. 3, p. 189–220.

Lebedeva, N.K., Aleksandrova, G.N., Shurygin, B.N., Ovechkina, M.N., Gnibidenko, Z.N. Paleontological and magnetostratigraphic data on Upper Cretaceous and lower Oligocene from borehole no. 8 (Russkaya Polyana District, Southwestern Siberia). Stratigraphy and Geological Correlation, v. 21, p. 48–78, 2013.

Lees, J. A., Bown, P. R., and Mattioli, E: Problems with proxies? Cautionary tales of calcareous nannofossil paleoenvironmental indicators. Micropaleontology , 51, 333–343., 2005.

Lehmann, M. F., Bernasconi, S. M., Barbieri, A., and McKenzie, J. A. Preservation of organic matter and alteration of its carbon and nitrogen isotope composition during simulated and in situ early sedimentary diagenesis, *Geochim. Cosmochim. Acta*, **66**, 3573–3584, 2002.

Lentin, J.K., Vozzhenikova, T.F. 1990: Fossil dinoflagellates from the Jurassic, Cretaceous and Paleogene deposits of the USSR — a re-study. American Association of Stratigraphic Palynologists, Contributions Series, no. 23, 241 p., pls. 1–16, 1990.

Li, L., and Keller, G: Maastrichtian climate, productivity and fauna turnovers in planktic foraminifera in South Atlantic DSDP sites 525A and 21. In Marine Micropaleontology (Vol. 33), 1998.

Linnert, C., Robinson, S. A., Lees, J. A., Bown, P. R., Pérez-Rodríguez, I., Petrizzo, M. R., Falzoni, F., Littler, K., Arz, J. A., and Russell, E. E.: Evidence for global cooling in the Late Cretaceous, *Nat. Commun.*, **5**, 4194, https://doi.org/10.1038/ncomms5194, 2014.

MacLeod, K. G: Extinction of inoceramid bivalves in Maastrichtian strata of the Bay of Biscay region of France and Spain. Journal of Paleontology, 68(5), 1048–1066. https://doi.org/10.1017/S0022336000026652, 1994.

Martini, E: Standard palaeogene calcareous nannoplankton zonation. Nature, 226(5245), 560–561. https://doi.org/10.1038/226560a0, 1971.

Masure, E., Rouse, P., et al. Fossil dinoflagellates from the Maastrichtian and Paleocene of the upper Cote d'Ivoire-Ghana Transform margin, 599, 960, 961, and 962, Proceedings of the Ocean Drilling Program, Scientific Results, volume 159, College Station, Texas, p. 253–276, 1999

https://doi.org/10.5194/egusphere-2026-3135
Preprint. Discussion started: 7 July 2026

McLachlan, S.M., Spero, A.V., Hebda, R.J. Dinoflagellate cysts from the upper Campanian (Upper Cretaceous) of Hornby Island, British Columbia, Canada, with implications for Namurian Group biostratigraphy and paleoenvironmental reconstructions. Marine Micropaleontology, v. 145, p. 1–20, 2018.

Meilijson, A., Ashckenazi-Polivoda, S., Ron-Yankovich, L., Illner, P., Alsenz, H., Speijer, R. P., Almogi-Labin, A., Feinstein, S., Berner, Z., Püttmann, W., and Abramovich, S: Chronostratigraphy of the Upper Cretaceous high productivity sequence of the southern Tethys, Israel. Cretaceous Research, 50, 187–213. https://doi.org/10.1016/j.cretres.2014.04.006, 2014.

Messaoud, J. H., Kalifi, A., Alibrahim, A., Ibrahim, K., Chirakal, T., Ardila-Sanchez, M., Leila, W. A., Chabaane, N. Ben, Grélaud, C., Powell, J. H., and van Buchem, F: Chronostratigraphy of the mixed Upper Cretaceous deposits at the northern margin of the Arabian Plate (Jordan). Newsletters on Stratigraphy, 58(2), 161–201. https://doi.org/10.1127/nos/2025/0858, 2025.

Meyers, P. A., Bernasconi, S. M., and Forster, A: Origins and accumulation of organic matter in expanded Albian to Santonian black shale sequences on the Demerara Rise, South American margin. Organic Geochemistry, 37, 1816–1830., 2006.

Moir, B.A., Mao, Shiao, 1997: Maastrichtian scleractinian corals from the Maud Rise and Gergis Basin (Southern Ocean): their stratigraphic and paleoenvironmental implications. Palaeogeography, Palaeoclimatology, Palaeoecology, v. 21, p. 41–56.

Moshkovitz, S., Ehrlich, A., Soudry, D., and Soudry Siliceous Microfossils, D: Siliceous Microfossils of the Upper Cretaceous Mishash Formation, Central Negev, Israel. In Cretuceous Research (Vol. 4)., 1983.

Müser, H.S., Mersch, C., 2002: A new biostratigraphic scheme for the Paleocene onshore western Greenland and its implications for the timing of the pre-volcanic evolution. Geological Society, London, Special Publications, v. 197, p. 111–156.

Nifuku, K., Kodama, K., Shigeta, Y., and Naruse, H: Faunal turnover at the end of the Cretaceous in the North Pacific region: Implications from combined magnetostratigraphy and biostratigraphy of the Maastrichtian Senpohshi Formation in the eastern Hokkaido Island, northern Japan. Palaeogeography, Palaeoclimatology, Palaeoecology, 271(1–2), 84–95. https://doi.org/10.1016/j.palaeo.2008.09.012, 2009.

Olde, K., Jarvis, I., Pearson, M., Wilden, J., Tocher, B., Trubov, A. 2015: A revised Northern European Upper Cretaceous to Eocene dinoflagellate cyst zonation. Palynology, v. 39, no. 2, p. 149–178.

Ovechkina, M. N., and Alekseev, A. S: Quantitative changes of calcareous nannoflora in the Saratov region (Russian Platform) during the late Maastrichtian warming event. J. Iber. Geol. , 31, 149–165., 2005.

Perch-Nielsen, K: Cenozoic calcareous nannofossils. Plankton Stratigraphy., 427–554., 1985.

Piasecki, L., Larsen, L.M., Pedersen, G.K. Palynostratigraphy of the Lower Tertiary volcanics and marine clastic sediments in the southern part of West Greenland Basin: implications for the timing and duration of the volcanism. Rapport Grønlands Geologiske Undersøgelse, v. 154, p. 13–31, 1992

Popelova, V., Chum, G.L., Walter, H.A. Environmental factors influencing the spatial distribution of dinoflagellate cyst assemblages in shallow lagoons of southern New England (USA). Review of Palaeobotany and Palynology, v. 128, p. 7–34, 2004

Powell, A.J. Dinoflagellate cysts of the Tertiary System. In: Powell, A.J. (editor), A Stratigraphic Index of dinoflagellate cysts, British Micropaleontological Society Series, London, UK, p. 155–229, 1992

https://doi.org/10.5194/egusphere-2026-3135
Preprint. Discussion started: 7 July 2026

Powell, J. H., and Moh', B. K: Evolution of Cretaceous to Eocene alluvial and carbonate platform sequences in central and south Jordan. GeoArabia, 16(4), 29–82. http://pubs.geoscienceworld.org/geoarabia/article-pdf/16/4/29/5445667/powell.pdf, 2011.

Prince, I.M., Jarvis, I., Pearce, M.A., Tocher, B.A. Dinoflagellate cyst biostratigraphy of the Coniacian–Santonian (Upper Cretaceous): New data from the English Chalk. Review of Palaeobotany and Palynology, v. 150, p. 59–96, 2008

Püttmann, and Tobias: Exceptionally well-preserved calcareous nannofossils from a late cretaceous nearshore setting : implications for stratigraphy and paleoecology., 2021.

Püttmann, T., Linnert, C., Dölling, B., and Mutterlose, J: Deciphering Late Cretaceous (Cenomanian to Campanian) coastline dynamics in the southwestern Münsterland (northwest Germany) by using calcareous nannofossils: Eustasy vs local tectonics. Cretaceous Research, 87, 174–184. https://doi.org/10.1016/j.cretres.2017.07.005, 2018.

Radmacher, W., Mangold, D., Tyszka, J. Dinoflagellate cyst biostratigraphy of Upper Cretaceous strata from two wells in the Norwegian Sea. Review of Palaeobotany and Palynology, v. 216, 18–34, 2015

Razmjooei, M. J., Thibault, N., Kani, A., Dinarès-Turell, J., Pucéat, E., and Chin, S: Calcareous nannofossil response to Late Cretaceous climate change in the eastern Tethys (Zagros Basin, Iran). Palaeogeography, Palaeoclimatology, Palaeoecology, 538(July 2019), 109418. https://doi.org/10.1016/j.palaeo.2019.109418, 2020.

Schwarz, W., Schröder, L.G. Fish otoliths from the latest Maastrichtian Kempl Clay (Texas, USA) and the early Danian Clayton Formation (Arkansas, USA) and an assessment of extinction and survival of teleost lineages across the K-Pg boundary based on otoliths. Rivista Italiana di Paleontologia e Stratigrafia, v. 126, no. 2, p. 395–446, 2020

Sissingh, W: Biostratigraphy of Cretaceous calcareous nannoplankton. GeologieenMijnbouw, 56, 37–65., 1977.

Sivankova, S.K. Dinozavt biostratigraphic of Santonian–Maastrichtian formations of the western Gulf Coastal Plain, southern United States. The Palaeontologist, v. 42, no. 3, p. 246–262, pls. 1–5, 1995

Sweeney, C.S., Sullivan, E.C. Stratigraphy and sedimentology of the Upper Cretaceous (Campanian) Anachoco Limestone, Texas USA. Cretaceous Research, v. 25, p. 473–497, 2004

Thibault, N: Calcareous nannofossil biostratigraphy and turnover dynamics in the late Campanian-Maastrichtian of the tropical South Atlantic. Revue de Micropaleontologie, 59(1), 57–69. https://doi.org/10.1016/j.revmic.2016.01.001, 2016.

Thibault, N., and Gardin, S: Maastrichtian calcareous nannofossil biostratigraphy and paleoecology in the equatorial atlantic (demerara rise, ODP leg 207 hole 1258A). . Rev. Micropaleontol, 49(4), 199–214., 2006a.

Thibault, N., Anderskouv, K., Bjerager, M., Boldreel, L. O., Jelby, M. E., Stemmerik, L., and Surlyk, F.: Upper Campanian–Maastrichtian chronostratigraphy of the Skælskør-1 core, Denmark: correlation at the basinal and global scale and implications for changes in sea-surface temperatures, *Lethaia*, **48**, 549–560, 2015.Thibault, N., and Husson, D: Climatic fluctuations and sea-surface water circulation patterns at the end of the Cretaceous era: Calcareous nannofossil evidence. Palaeogeography, Palaeoclimatology, Palaeoecology, 441, 152–164. https://doi.org/10.1016/j.palaeo.2015.07.049, 2016.

Thierstein, H. R. ,: Late Cretaceous nannoplankton and the change at the Cretaceous- Tertiary boundary. In J. E. Warme, R. G. Douglas, & E. L. Winterer (Eds.), The Deep Sea Drilling Project: a Decade of Progress (Vol. 32, pp. 355–394). Society of Economic Paleontologists and Mineralogists, Special Publication., 1981.

https://doi.org/10.5194/egusphere-2026-3135
Preprint. Discussion started: 7 July 2026

1182 Thom, V., Riding, J., Francis, J. The Late Cretaceous dinoflagellate cyst Manumiella — biostratigraphy, systematics
1183 and palaeoecological significance. Review of Palaeobotany and Palynology, v. 156, p. 436–448, pls. 1, 2, 2009

1184 Tocher, B.A. Campanian to Maastrichtian dinoflagellate cysts from the United States Atlantic Margin, Deep Sea
1185 Drilling Project, Site 612, Deep Sea Drilling Project, Initial Reports, U.S. Government Printing Office, College
1186 Station, Texas, p. 419–428, 1987

1187 Twichell, S. C., Meyers, P. A., and Diester-Haass, L: Significance of high C/N ratios in organic-carbon-rich Neogene
1188 sediments under the Benguela Current upwelling system. Organic Geochemistry, 33(7), 715–722., 2002.

1189 Usman, M., Ardila-Sanchez, M., Idiz, E., Abu-Mahfouz, I. S., van Buchem, F., and Vahrenkamp, V: Organic and
1190 inorganic geochemical cyclicity of a Maastrichtian oceanic open-shelf carbonate source rock. Scientific Reports,
1191 15(1). https://doi.org/10.1038/s41598-025-99832-w, 2025.

1192 Voigt, S., Gale, A. S., Jung, C., and Jenkyns, H. C.: Global correlation of Upper Campanian–Maastrichtian successions
1193 using carbon-isotope stratigraphy: development of a new Maastrichtian timescale, *Newsl. Stratigr.*, 45**,** 25–53,
1194 2012.

1195 Watkins, D. K: Upper cretaceous nannofossils from leg 120, kerguelen plateau, southern ocean. Proc. Ocean Drill.
1196 Program Sci, 120, 343–370., 1992.

1197 Williams, G.L., Brinkhuis, H., Pearce, M.A., Fensome, R.A., Weegink, J.W. Southern Ocean and global dinoflagellate
1198 cyst events calibrated: Index events for the late Cretaceous–Neogene. In: Exon, N.F., Kennett, J.P., & Malone,
1199 M.J. (editors), Proceedings of the ODP, Scientific Results, volume 189, College Station, Texas, p. 1–98, 2004.

1200 Williams, G.L., Stover, L.E., Kidson, E.J. Morphology and stratigraphic ranges of selected Mesozoic–Cenozoic
1201 dinoflagellate taxa in northern Hemisphere, geological Survey of Canada, Paper, 92, p. 1–40, 1993

1202 Wise, S. W: Mesozoic and cenozoic calcareous nannofossils recoveredby deep sea drilling project leg 71 in the
1203 falkland plateau region, south-west atlantic ocean. . Initial Rep. Deep Sea Drill. Proj, 71, 481–550., 1983.

1204

1205

1206